



UNIVERSITY OF NAIROBI

**ASSESSMENT OF NON-IONIZING RADIATION EXPOSURE
LEVELS IN SELECTED COMMERCIAL AND RESIDENTIAL
AREAS OF NAIROBI CITY**

BY

WACHIRA REUBEN CHIIRA

S56/12576/2018


BSc (Hons), Physics

A Thesis Submitted in Partial Fulfillment of the Requirements for Award of the Degree of
Master of Science in Nuclear Science of the University of Nairobi.

© August, 2022

DECLARATION

This thesis is my original work and has not been presented for a degree in any other university

Signature:  Date: 16th August 2022

Wachira Reuben Chiira

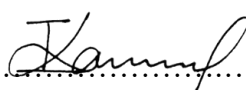

S56/12576/2018

Department of Electrical and Information Engineering

Faculty of Engineering

University of Nairobi

This thesis is submitted for examination with our approval as research supervisors:

	Signature	Date
Dr. M. I. Kaniu Department of Physics University of Nairobi P.O Box 30197-00100, Nairobi, Kenya. ikaniu@uonbi.ac.ke	 18-08-2022
Prof. M. J. Gatari Department of Electrical & Information Engineering University of Nairobi P.O Box 30197-00100, Nairobi, Kenya. mgatari@uonbi.ac.ke	 18 August 2022

DEDICATION

This work is dedicated to my family members for all the support towards my life.

ACKNOWLEDGEMENT

My work would not have been a success without support from various individuals who were always ready to assist me through this journey. I thank God for giving the grace to work on my thesis. Without Him I wouldn't have made it.

I highly appreciate my supervisors Dr. M. I. Kaniu and Prof. M. J. Gatari for walking along this journey of research and writing thesis with me. It is through their professional guidance and support that I was able to do this project. In case of any challenge, you were always ready to intervene and see me succeed. I highly appreciate Mr J. K. Chumba and the Kenya Nuclear Regulatory Authority management for helping with the right equipment for outdoor RF measurements. I extend sincere thanks to Mr. M. Mailu and Mr. S. Bartilol of the Institute of Nuclear Science & Technology (INST) for assisting me with the necessary components needed for the equipment to function. Worthy of appreciation is Mr. Moses Kinyanjui for guiding me on how to use the Spectran equipment. I will forever be grateful to Mr. C. N. Ndung'u who was always present for consultation on using R software during data analysis work.

Special thanks to fellow students from INST, Department of Electrical & Information Engineering and Department of Physics for encouragements and advice throughout the time I was working on my thesis.

Sincere gratitude also goes to my wife and the other family members for the social and financial support and encouragement that they accorded me. Special thanks to you all for your support and care.

May the good Lord bless you all.

ABSTRACT

Assessment of non-ionizing radiation (NIR) exposure levels in both urban and rural areas is necessary owing to the vast utilization of wireless communication and associated devices that utilize radio-frequency energies. Excessive NIR exposure has been linked to negative human health effects such as nerve stimulation and changes in cell membrane permeability. The International Commission for Non-Ionizing Radiation Protection (ICNIRP) provides NIR exposure guidelines for both occupational workers and the general public. The city of Nairobi is the headquarters for many telecommunication companies in Kenya, and it is densely populated. Thus, many base transmission stations (BTS) have been installed by various telecommunication providers. However, there has been no scientific study undertaken so far to assess the NIR exposure levels. This work provides a preliminary study of NIR exposure levels to the general public in Nairobi. Electromagnetic frequency fields (EMF) were measured systematically using a spectrum analyzer (Spectran HF6065) connected to an antenna (HyperLOG 7060) in the city's Central Business District (CBD) and in three densely populated areas at the outskirts of the CBD. The observations were assessed and compared with the ICNIRP standards. The median values for the total exposure to EMF in Nairobi CBD and residential areas were 0.90 ± 0.30 V/m and 0.81 ± 0.25 V/m respectively, while the total exposure values to EMF range 0.14 V/m and 3.67 V/m. The GSM900 was found to contribute higher exposure to NIR than the other frequency bands (LTE700, LTE800, GSM1800, UMTS2100 and LTE2600) considered in this work. Using the Kriging technique, a spatial map showing the distribution of the EMF measurements was generated showing areas with high probability of EMF exceeding 2 V/m in the CBD. The results obtained showed that the exposure to EMF in all the areas assessed was below the limits provided by the ICNIRP guidelines. The findings of this study can be used to establish a baseline for future NIR exposure studies.

Keywords: *BTS, EMF, Kriging, NIR exposure, Nairobi city*

TABLE OF CONTENTS

DECLARATION	ii
DEDICATION	iii
ACKNOWLEDGEMENT	iv
ABSTRACT	v
LIST OF FIGURES	ix
LIST OF TABLES	x
LIST OF ABBREVIATIONS & ACRONYMS	xi
CHAPTER ONE: INTRODUCTION	1
1.1 Background to the Study	1
1.2 Statement of the Problem	2
1.3 Objectives	2
1.3.1 General Objective	2
1.3.2 Specific Objectives	2
1.4 Justification and Significance of the Study	3
1.5 Thesis Organization	3
CHAPTER TWO: LITERATURE REVIEW	5
2.1 Chapter Overview	5
2.2 Interactions of RF-EMFs with the Human Body	5
2.3 Survey of NIR Exposures around the World	6
2.4 Methods and Techniques Used in RF-EMF Measurements	7
2.5 Visual Representation of RF-EMF Exposure Measurements	9
2.6 Research Gaps	11
CHAPTER THREE: THEORETICAL BACKGROUND	12
3.1 Chapter Overview	12
3.2 Assessment of High-frequency Electromagnetic Fields	12
3.3 Analysis Techniques for Electromagnetic Fields	15

3.3.1 Statistical Analysis of Electromagnetic Fields	15
3.3.2 Exploratory Data Analysis of Electromagnetic Fields.....	19
3.4 Geostatistical Techniques for Mapping RF Measurements	19
3.5 Assessing the Electric Field Exposure for ICNIRP Compliance	22
CHAPTER FOUR: METHODOLOGY	23
4.1 Chapter Overview	23
4.2 Measurement of RF-EMF Exposure Levels.....	23
4.2.1 Aaronia Spectran HF-6065 Used for Measurements of Electric Field	23
4.2.2 Parameters Considered in the RF-EMF Measurements	24
4.2.3 Sites Considered for the RF-EMF Exposure Survey	25
4.3 Analysis of the RF-EMF Exposure Measurements.	30
4.4 Spatial Interpolation of the RF-EMF Measurements.....	32
CHAPTER FIVE: RESULTS AND DISCUSSION	34
5.1 Chapter Overview	34
5.2 Results of RF-EMF Exposure Measurements	34
5.2.1 RF-EMF Levels in Residential Areas	36
5.2.2: RF-EMF Levels in the CBD.....	37
5.3 Results of Variability Assessment of RF-EMF Levels and Comparison with ICNIRP Values	38
5.3.1 Comparison of residential and CBD RF-EMF measurements	44
5.3.2 Comparison of the measured RF-EMF values with ICNIRP guidelines	45
5.3.3 Exploratory Analysis of RF-EMF Data	45
5.4 Results of Geospatial Mapping of RF-EMF Levels in the CBD.....	49
CHAPTER SIX: CONCLUSION AND RECOMMENDATIONS	53
6.1 Conclusion.....	53
6.2 Recommendations.....	54

REFERENCES	55
APPENDICES	61
Appendix 1: R Code for Kriging	61
Appendix 2: R Code for PCA	79
Appendix 3: Summary of CBD Electric Field Values for Various Bands	84

LIST OF FIGURES

Fig. 4.1: Spectrum Analyzer connected to a PC	24
Fig. 4.2: Illustration of EMF measurement points in residential areas	28
Fig. 4.3: Nairobi CBD map with labelled points where EMF measurements were done.....	30
Fig. 5.1: Typical spectrum showing various bands used for telecommunication services.....	34
Fig. 5.2: The electric field variations for various frequencies at the time of sampling.	35
Fig. 5.3: Variation of the total electric field in a residential building in site 3.....	39
Fig. 5.4: Histogram of electromagnetic field distribution in CBD region.....	43
Fig. 5.5: Total exposure levels at various positions in Nairobi CBD	45
Fig. 5.6: Boxplot of median values of electromagnetic field exposure in CBD and residential areas.....	46
Fig. 5.7: Graphical representations of empty regions.....	47
Fig. 5.8: (a) PCA scores plot and (b) PCA loadings plot for the residential and CBD EMF exposure.....	48
Fig. 5.9: S-plot for (a) PC1 and (b) PC2.....	49
Fig. 5.10: Variogram model used for kriging.....	50
Fig. 5.11: Map of Nairobi CBD indicating (a) interpolated values of RF-EMF exposure and (b) variance of the interpolated EMF measurements.....	51
Fig. 5.12 (a): Photos of the three sites that exhibited the highest RF-EMF exposure levels.....	52
Fig. 5.13: Map of Nairobi CBD indicating the probability of RF-EMF exceeding 2 V/m.....	53

LIST OF TABLES

Table 1.1: EMF exposure reference levels for the general public (ICNIRP, 2020)	2
Table 4.1: Cellular phones operating frequency bands (Source: CAK, 2019)	25
Table 4.2: Description of identified sites for NIR assessment.....	26
Table 5.1: Summary statistics of different residential areas.....	38
Table 5.2: Descriptive statistics for the total electric field in the CBD region.....	39
Table 5.3: Summary of the frequency bands in the residential areas.....	42
Table 5.4: Variation of electric field at various distances and directions.....	43
Table 5.5: Electromagnetic field for various bands in Nairobi CBD.....	44
Table 5.6: Summary of sites with elevated levels of exposure to EMF fields.	52

LIST OF ABBREVIATIONS & ACRONYMS

BTS	Base Transmitter Station
CAK	Communications Authority of Kenya
CBD	Central Business District
EDA	Exploratory Data Analysis
EMF	Electromagnetic Field
FM	Frequency Modulation
GPS	Global Positioning System
GSM	Global System for Mobile Communications
ICNIRP	International Commission for Non-Ionizing Radiation Protection
IDW	Inverse Distance Weighted
ITU	International Telecommunication Union
KNBS	Kenya National Bureau of Statistics
LTE	Long Term Evolution
MCS	Multipoint Communication System
NIR	Non-Ionizing Radiation
PCA	Principle Component Analysis
RF	Radiofrequency
RMS	Root Mean Square
SA	Spectrum Analyzer
SMA	Sub-Miniature version A
UMTS	Universal Mobile Telecommunications Service

CHAPTER ONE

INTRODUCTION

1.1 Background to the Study

NIR is any emission in the electromagnetic spectrum with inadequate energy per quantum to dislodge an electron from a molecule or an atom (Maxwell, 1998). Different types of NIR, namely visible light, radiofrequency, ultraviolet, and infrared, have unique properties that inform the rationale for their uses. NIR may either ensue from human activities or exist naturally. The most prevalent artificial sources of NIR include high-voltage power cables, base transmitter stations (BTS), radar systems, and other appliances such as mobile phones and microwave ovens. Regular application of radiofrequency (RF) energy (otherwise known as RF radiation) in telecommunication technology comprises the most widespread application of NIR. The frequency of RF radiation generally ranges from 3 kHz to 300 GHz and is essential for remote signal transmission. All RF frequencies greater than 300 MHz are referred to as microwaves. This range is appropriate for large bandwidth broadcasting such as radar signals, cellular phones, and satellite communications.

The wireless network technology has since replaced cables in signal transmission due to its cheaper installation and maintenance cost. Devices using wireless technologies are connected through the omnidirectional or directional (covers a typical azimuth of 120 degrees) antenna (Lopa and Vora, 2015). The efficacy of these technologies is subject to the quality of signals being received from the closest cellular towers and the number of devices connected (Saravanamuttu *et al.*, 2015). Hence, telecommunication service providers install as many BTS as required to reduce traffic on a particular network.

Human exposure to time-varying electromagnetic fields (EMF) that exceed particular thresholds has been found to cause adverse health effects (Câmara, 2014). In this regard, the International Commission for Non-Ionizing Radiation Protection (ICNIRP) provides NIR exposure guidelines for both occupational workers and the general public (ICNIRP, 2020). These guidelines specify basic restrictions and reference levels for time-varying EMF. It is the reference levels that are used for practical exposure assessment to show whether acceptable levels have been exceeded. Evaluation of exposure (near and far-field

zones) requires the knowledge of the magnetic field (B), magnetic field strength (H), electric field strength (E), and power flux density (S), as indicated in Table 1.1. Within the context of this study only the general public exposure was considered.

Table 1.1: EMF exposure reference levels for the general public (Source: ICNIRP, 2020)

Frequency Range	Incident E-field Strength E_{inc} (V/m)	Incident H-field Strength H_{inc} (A/m)	Incident power density S_{inc} (W/m^2)
0.1-30 MHz	$300/f_M^{0.7}$	$2.2/f_M$	N/A
>30-400MHz	27.7	0.073	2
>400-2000 MHz	$1.375f_M^{0.5}$	$0.0037f_M^{0.5}$	$f_M/200$
>2-6GHz	NA	NA	10

f_M is the frequency in MHz

N/A denote ‘not Applicable’ and is not necessary when assessing compliance.

1.2 Statement of the Problem

There has been an increased application of RF energy in Kenya in the recent past. A report released in 2019 showed that Kenya had more than 46 million internet users and 51 million active mobile subscribers (CAK, 2020) . Therefore, Nairobi being the most populous city, according to the recent census report by the KNBS, (2019) is likely to have the highest NIR exposure levels. This situation necessitates a continuous assessment of NIR exposure to ascertain that the exposure limits are not exceeded. Furthermore, no scientific study has been undertaken so far to assess the NIR exposure levels.

1.3 Objectives

1.3.1 General Objective

The main focus of this research was to assess the status of NIR exposure caused by RF-EMF in selected commercial and residential areas of Nairobi City.

1.3.2 Specific Objectives

The specific objectives of the study were:

- (i) To establish the NIR levels for residential and commercial areas in Nairobi City based on time-varying EMF measurements within 300 m radius from BTS and other communication devices.
- (ii) To assess the variability of EMF measurements in different sites from (i) above using statistical and exploratory data analysis techniques, and compare the results with ICNIRP guidelines.
- (iii) To generate a geospatial map showing distribution of RF-EMF levels for Nairobi CBD using the Kriging technique.

1.4 Justification and Significance of the Study

There are limited studies on the status of exposure to RF-EMF in Kenya despite the increased use of NIR sources. Several studies have reported cases of adverse human health effects associated with the overexposure of time-varying EMF and warrant the assessment of NIR (Yakymenko *et al.*, 2011). Although studies on the impacts of prolonged exposure to NIR have not reached a common conclusion, the short-term effects of NIR on biological tissues have been validated (ICNIRP, 2020).

Using a theoretical approach in the characterization of RF-EMF exposure is incredibly intricate due to the existence of many variables in a given area. Subsequently, there is a need to perform measurements in a particular region and identify the possible sources of RF-EMF radiation. At the time of the study, there was limited availability of empirical data from cellular towers in Kenya that could be used to model NIR exposure levels. The results obtained from this work are thus useful in informing NIR protection guidelines by the relevant authorities. Furthermore, this work provides the baseline measurements for future NIR exposure studies.

1.5 Thesis Organization

This thesis has been organized into five chapters. Chapter one is the introduction with background information about NIR, the main challenge that needed to be addressed and justification of the study. Chapter two constitutes the literature review of the previous studies relevant to the current work. The chapter explores the methods and materials used

by other researchers in different parts of the world and the results obtained. This chapter informs the most appropriate techniques and equipment needed for assessment of NIR exposure. Chapter three comprises the knowledge of theoretical principles necessary for measurement and analysis of NIR. The procedures and equipment used for the measurement of electric field and analysis of the data is provided in chapter four. The results of the electric field measurements are discussed in chapter five. It includes the exploratory data and statistical analysis results. It also provides the mapping of the NIR data. Lastly, chapter six provides the conclusions of the study and further work that needs to be done.

CHAPTER TWO

LITERATURE REVIEW

2.1 Chapter Overview

This chapter provides a review of the previous studies related to RF-EMF assessment. It presents the findings of the studies and various methods used in the measurement, analysis, and representation of the RF-EMF exposure data. Finally, these studies informed the approaches that were employed in the study.

2.2 Interactions of RF-EMFs with the Human Body

The oscillating magnetic and electric fields transfer energy from the RF-EMF source to objects within their propagation paths. When these fields interact with the biological tissue, their power is either reflected away or absorbed (ICNIRP, 2020). This interplay results in a complex system of electromagnetic fields in the tissues that depend on the properties of EMFs, physical characteristics, and body dimensions. The absorbed electric fields are referred to as induced electric fields (E_{ind}) and have adverse health impacts on human tissues. Once inside the body, the E_{ind} exerts a force on both free-moving particles such as ions and electrons and polar molecules. These interactions lead to the conversion of EMF energy to kinetic energy, making the charged particles move as current and the polar molecules to rotate. Consequently, heat that affects tissues in various ways is generated. The E_{ind} can also exert sufficient force to induce the dielectric breakdown of biological membranes.

Furthermore, electromagnetic fields of up to 10 MHz can trigger nerve stimulation in the body. This effect is dependent on the frequencies and is generally described as “tingling” sensation. Increasing the frequency of the EMF field entering the body leads to temperature rise and the nerve stimulation impacts reduce (ICNIRP, 2020). Interaction of electromagnetic fields with tissues alters cell membrane permeability. Pulsing a sufficiently intense EMF in to the body induces cellular changes including permeability of cell membranes. These aspects of the RF-EMF inform the ICNIRP when establishing the guidelines for the exposure to NIR.

There are various sources of NIR in the world that either exist naturally or artificially generated. Cell phones and radio emitters are among the sources of radiofrequency and

microwaves, and can damage body tissues through heating at high intensities. High-voltage powerlines, electrical wiring and equipment also produce NIR. Infrared lasers, furnaces and headlamps generates NIR that causes heat sensation and pain to the body. UV lasers, the sun and welding arcs are among the sources of ultra violet radiation. The majority of the RF-EMF studies around the world show that telecommunication structures and devices are the primary sources of NIR exposure, followed by FM and TV broadcasting (Sagar *et al.*, 2018).

2.3 Survey of NIR Exposures around the World

Researchers in different parts of the world used various techniques to assess the levels of exposure to NIR. A study by Joseph *et al.*, (2010) investigating the NIR exposure in different European countries, namely Slovenia, Belgium, Hungary, Netherlands, and Switzerland, found that up to 97 % of exposure in public transport such as buses came from wireless telecommunication devices. A similar study in Australia reported that downlink frequency contributed up to 40 percent, followed by broadcast that led to 22.4 % of the NIR exposure (Zelege *et al.*, 2018). FM broadcast and GSM 900 were reported as the main contributors of NIR exposure in Belgium, while the major sources of RF radiation in Greece were GSM 1800 and 3G network (Vermeeren *et al.*, 2013). A radiofrequency radiation assessment in Switzerland reported that 67.2 % of the exposure resulted from mobile phone use, and 19.8 % came from mobile phone base stations. LTE 800 MHz, GSM 1800 MHz, and GSM 900 MHz were reported as the main contributors of radiofrequency radiation exposure in Turkey (Kurnaz and Korunur Engiz, 2016). Nonetheless, the measured values in all the places were within the acceptable limits as provided by the ICNIRP.

The RF radiation exposure studies from different regions showed that the exposure varies significantly based on network traffic in various environments. Working places in Slovenia recorded the highest exposure values ($255.0 \mu\text{W}/\text{m}^2$) (Gajsek *et al.*, 2016). These values were significantly low compared to the recommended limits, which is approximately $4.5 \text{ W}/\text{m}^2$ for a source radiating at a frequency of 900 MHz. Chiaramello *et al.*, (2019) analyzed the reports of the RF-EMF exposure published within a period of ten years and found that offices had the highest values probably due to outdoor and indoor sources of radiofrequency radiation. Another study comparing NIR exposure from various

parts of the world, namely, South Africa, Switzerland, Australia, Nepal, Ethiopia, and the United States of America, showed that RF radiation exposure in urban areas was mostly higher than in rural areas (Sagar *et al.*, 2018). Generally, most studies reported that downlink frequencies that dominate the outdoor environment were the main contributors to NIR exposure.

According to the findings of various studies worldwide, including African countries such as Ethiopia, South Africa, and Nigeria, multiple factors influence RF radiation exposure and should be considered during NIR exposure assessment. However, such studies are limited in Kenya, and the status of exposure to NIR, particularly due to the recent advancement in wireless telecommunication technology, remains unknown. Therefore, measurement of exposure due to BTS and FM and TV broadcast systems could give crucial information on the status of RF exposure. Furthermore, during NIR assessments, outdoor environments appeared to be the most appropriate regions to consider.

2.4 Methods and Techniques Used in RF-EMF Measurements

The three methods widely used for collecting outdoor RF-EMF field exposure data are: drive test measurement, spot measurement, and theoretical calculations (ITU, 2015). The drive test method constitutes an ongoing collection of RF-EMF exposure values from a moving car with data collection equipment. Using a GPS, simultaneous physical positioning and measurements can be achieved. This approach has been found to be useful for large area NIR exposure assessments (Kurnaz and Korunur Engiz, 2016). However, drastic movements of the vehicle have been reported to cause effects on the electromagnetic fields that lead to wrong measurements (ITU, 2015). Hence, it is vital to avoid potholes where possible and move at low speed. This data collection method is considered as being prone to erroneous results and thus requires additional spot measurements to meet the requirements provided by ICNIRP and other international bodies.

Spot measurements of the RF-EMF exposure level have been reported to provide an effective and systematic way of assessment using a grid method. This approach requires a subdivision of the area into polygons whose sides do not exceed 500 m. It has been found that this distance allows typical samples of all possible sources and, in every direction, to

be considered (Aerts *et al.*, 2013). Spot measurements can then be measured at the vertices of the polygons. Using this approach during NIR exposure data collection has been found to overcome the challenges of sudden movement in static fields as in the drive test.

Theoretical calculations involve models based on known parameters of the transmission antennas and are easier than other methods. (Rowley and Joyner, 2012). However, the exposure pattern may not be easily achieved in a complex environment. Electromagnetic waves can be reflected or absorbed by various structures, hence limiting this method. It may also give wrong exposure levels since it uses the worst-case scenario in approximating the exposure levels. This method performs better when combined with other methods (ITU, 2015).

The RF-EMF measurements are usually collected at a fixed location or mobile-based, using personal dosimeter, which provide a method of collecting multitudes of measurements in a simplified way (Rowley and Joyner, 2012). However, the use of personal exposure meter in assessing outdoor exposure to RF-EMF has been found to have some limitations. For instance, these devices have limited sensitivity and may give erroneous results due to unwarranted interactions with the operator. Using personal dosimeter is also considerably more expensive and time-consuming for long-term measurements and extensive studies because they give information based on personal exposure rather than that of a particular location.

Broadband meter provides a more effective way of collecting total NIR exposure data in a given area. However, broadband meter cannot be used for the channel- or frequency-specific RF-EMF exposure measurements (Buckus *et al.*, 2017). Therefore, any study that aims to assess NIR exposure from given frequencies requires an additional assessment using spectrum analyzers (SA). The utilization of SA in collecting RF-EMF exposure data at a fixed position offers the most accurate way of RF-EMF measurement (Buckus *et al.*, 2017). Nonetheless, SA is time-consuming compared to broadband meter since the frequency bands are evaluated independently. Also, it is an expensive method that requires an expert in that field.

Some studies have employed both broadband and narrowband frequency meter to assess RFEMF exposure levels. Aerts *et al.* (2013) used an NBM-550 broadband meter to measure the value of total NIR exposure followed by frequency-selective analysis using a spectrum analyzer to identify the specific frequency band contributing to the exposure. Other studies used a spectrum analyzer to characterize the NIR exposure resulting from mobile phone base stations (Ajiboye and Osiele, 2013; Bin Khuzairi *et al.*, 2019). Where the frequency bands of the RFEMF to be assessed are known, SA has been found to be sufficient for NIR exposure measurements.

Other studies have been conducted to investigate how distance from a radiating antenna affects the electric field exposure. Buckus *et al.*, (2017) found that the values of measured RF-EMF power density reduced as the distance from source increased. Measurements were performed up to a distance of 500 m along the main lobe. The maximum value was measured at 50 m from the antennas and the values reduced constantly up to 100m. At longer distances than 100m, the value of power density kept on fluctuating between 0.05 and 0.1 $\mu\text{W}/\text{cm}^2$. In another study, Ozen *et al.*, (2007) found that the electric field intensity values were higher at distances less than 300 m from a BTS.

It may be concluded that methods and techniques used in NIR measurements affect the accuracy and reliability of the results. Therefore, these factors are thus used to inform the choice of equipment and data collection approaches. The spot measurement method was adopted in the study as it was more effective in preliminary NIR exposure surveys. Additionally, since possible NIR sources and their operating frequencies were known, the SA was used for RF-EMF measurements.

2.5 Visual Representation of RF-EMF Exposure Measurements

In order to present NIR measurements in a way that decision-makers (relevant safety regulatory authorities) can easily understand, methods such as heat maps and statistical graphs are required (Aerts *et al.*, 2013). Heat maps provide a more visual approach that can be used to describe RF-EMF exposure levels in rural, suburban, or urban areas. These maps are either constructed using non-measurement models or measurement-based simulators (Breckenkamp *et al.*, 2008). Measurement-based models allow for accuracy

enhancement by adding more measured values (Paniagua *et al.*, 2013). Hence, developing models based on measured values leads to more accurate heat maps.

Spatial interpolation is another method used to approximate measurements at a given location without actual measurements based on values obtained from measured points (Azpurua and dos Ramos, 2010). This technique is based on two fundamental assumptions; spatial autocorrelation and continuity of values over space (Wu and Hung, 2016). Interpolation of data employs inverse distance weighted (IDW), spline, and kriging techniques. It is often utilized as a geographical approach for spatial data visualization, spatial quarry, and spatial decision-making procedures in GIS and environmental studies (Aerts *et al.*, 2018).

Kriging is a stochastic technique that utilizes a linear combination of values at known points to approximate the unknown data values at a particular location (Matheron, 1971). Variogram, the function showing the spatial correlation measure of a stochastic process, is essential in kriging interpolation. This technique provides the degree of uncertainty of the estimated surface. However, it is more time-consuming than spline and IDW (Wu and Hung, 2016). The kriging technique has been widely applied in the interpolation of data spaces in ground profiles. Unlike the other methods, it provides more accurate results and minimum bias making it ideal for interpolating distantly scattered data (Aerts *et al.*, 2018; Meng *et al.*, 2013). Some studies comparing various interpolation techniques reported that kriging interpolation is better than the others (Bekele *et al.*, 2003; Meng *et al.*, 2013; Yao *et al.*, 2013).

The IDW is a more uncomplicated technique that uses a linear integration of close measured points to estimate the values of unmeasured points (Azpurua and dos Ramos, 2010). However, it has been found that it is sensitive to outliers and has no error indication (Ikechukwu *et al.*, 2017). Schloeder *et al.*, (2001) compared the performance of spline, IDW, and kriging interpolation methods and found that kriging and IDW had similar performance and were more accurate than spline interpolation. However, Mueller *et al.*, (2001) reported slight differences between kriging and IDW when the methods were applied in the study of soil properties. In a similar study, Kravchenko, (2003) concluded that the accuracy of interpolation techniques depends on the spatial structure.

In view of the above studies, any of the three methods can be used to interpolate RF-EMF data. However, kriging has been reported to produce better prediction and more accurate results with less bias compared to IDW and spline techniques. Hence, it was used in the study as the interpolation technique.

2.6 Research Gaps

There are several studies conducted with efforts to reveal the status of exposure to electromagnetic fields. Most of these studies have successfully reported the statistical and exploratory analysis results after actual measurements of the electromagnetic fields intensity. However, there are limited studies showing the hotspots regions with elevated values of electric field. Interpolation of the measured values of power density or electric field strength over a geographical map can be essential in showing the regions with high values of EMF exposure. Although there is rapid increase in the application of wireless technology in Kenya, there has been no regular assessment of NIR exposure. Mapping of the electric field data using geostatistical techniques, such as kriging, is thus required to assist in revealing the trends as well as hotspots of NIR exposure. Such studies, however, are currently unavailable in Kenya.

CHAPTER THREE

THEORETICAL BACKGROUND

3.1 Chapter Overview

This chapter provides an overview of the theoretical concepts supporting the assessment and analysis of EMF exposure data. It also explains the basic principles concerning the propagation of electromagnetic waves and factors affecting their transmission. Other concepts useful in data analysis and spatial interpolation of data are also included.

3.2 Assessment of High-frequency Electromagnetic Fields

The technologies used in telecommunications (telephony, television broadcasting, radar, etc) intend to facilitate the effective propagation of electromagnetic waves from the transmitter to the receiver. The primary idea of electromagnetic waves propagation is essential for estimating the ambient levels of EMF fields, regardless of their use. The magnetic field (H) and electric field E must exist simultaneously for a given wave to propagate across a considerable distance in relation to its wavelength (Staebler, 2017). The field is confined near the source if one of the two elements is absent.

The energy carried by electromagnetic waves is distributed across a progressively large area during propagation in a place with no obstacles (free space). Similarly, the wave energy per unit surface area decreases inversely with square of the distance from the source. The energy crossing a unit surface per unit of time is referred to as power density S (power per surface unit (W/m^2)), and its concept allows for the characterization of exposure at high frequencies. Power density, a product of electric and magnetic fields, is regarded as homogenous over a wide surface area (see equation 3.1) (Staebler, 2017). The magnetic and electric fields attenuate with distance, while the power density reduces with distance in the phenomenon of free space loss. This loss increases significantly with the presence of obstacles such as hills, structures, and plants.

$$S = E \times H \tag{3.1}$$

Where S is power per surface unit, E is electric field and H is magnetic field.

Telecommunication seeks to optimize the power irradiated with reference to power supplied. To achieve this, the transmitters are fitted with antennas appropriate for the

wavelength of the signal to be relayed. Antennas comprise a reversible reciprocal system (these features remain similar in reception and emission) and can transmit signals over a wide region or concentrate energy in a particular direction of interest. The intended direction of transmission is referred to as the main lobe while directions with lower levels of power irradiated are called side lobes. The main lobe is likely to contribute to higher exposure levels than the side lobes.

The characterization of electromagnetic fields requires knowledge of the nature of the fields in the region of consideration. The assessment of the near field is distinct from that of the far-field zone, and the border between the two zones depends on the parameters of the radiating structures in terms of wavelength. The waves in the far-field region (Fraunhofer zone) propagate according to well-defined characteristics; the electric and magnetic fields attenuate regularly with increasing distance, waves are considered planar, E and H remain orthogonal to each other and the path of propagation (Staabler, 2017). The field level and power density S at each point can easily be estimated and one of these elements (S, E or H) is sufficient to characterize the exposure.

However, the characterization of electromagnetic field exposure in the near field is complex. The electric field is based on how the electric charges are spread and the electric features of the elements present in that region while the magnetic fields depend on the current flow of the source (Staabler, 2017). These fields reduce with the square or cube of the distance and are neither in phase nor orthogonal. Their minima and maxima are not found at the same place and their strengths can differ considerably over small distances. Consequently, characterization of the exposure status in the near field region is only possible through numerical simulation due to the complexity of H and E fields distributions which makes it impossible to relate them using equations. Also, the presence of an obstacle including a measuring probe considerably alters the radiation levels, adding more assessment difficulties. Subsequently, the electric field must be measured separately from the magnetic fields. Using the far-field formula in the near field zone results in over estimation of field and power density levels. The total electric field requires the electric field associated with individual frequencies to be summed up using the expression shown by equation 3.2.

$$E_{Total} = \sqrt{\sum_{i=1}^n E_i^2} \quad 3.2$$

Where E_{Total} is the total electric field and E_i is the measured electric field ranging from 1 up to n where n is an integer.

The traffic channels from a base station are used to send signals only when required and may use power regulation systems. Therefore, the power emitted by the antenna may vary depending on the number of channels in use and the number of time slots in the traffic channels. The RF-EMF exposure is also likely to vary with the distance from the source (Mann *et al.*, 2000). Certain types of antennas radiate in all directions while others (sector antennas) radiate power in a particular direction, reducing interference and allowing re-use of frequencies. Subsequently, most base stations in high-traffic density regions use sector antennas. The sector antennas gain ranges between 10 and 20 dBi, which implies that the radiated power may be between 10-100 times stronger in the intended directions than omnidirectional antennas (Mann *et al.*, 2000).

The antenna lobe also has vertical directionality, with a reasonably narrow beam usually tilted slightly downward. The power intensity in the main lobe reduces with the square of the distance. However, the power variation on the ground is complex since the highest level is found at a distance where the main lobe reaches the ground. The power on the ground at distances near the antenna on a building or BTS may be considerably lower than in the main lobe. As the distances from the antennas increase, the presence of hills and buildings cause a substantial decrease in the irradiated power due to attenuation and or reflections of the power density. The leading cause of power decrease in the study regions can be attributed to the presence of buildings.

The magnetic and electric fields comprise the physical quantities assessed to establish high frequency EMF levels. The device used to assess high-frequency EMF fields is chosen based on the number of radiation sources, frequency domain to be assessed, and attributes of the radiation (Staebler, 2017). The primary constituents of the measuring system constitute a probe with at least one sensor, coaxial cables that transmit electric signals from the antennas, and the processing unit that converts received signals into quantities that can quantify the exposure.

The spectrum analyzer used in the assessment of the EMF exposure data consists of four operation modes, namely, broadband peak, exposure limit calculation, spectrum analysis, and audio output modes with settings to allow for the measurement of various variables, namely, power (dBm), electric field strength (V/m), power per unit area (W/m²), and magnetic field strength (A/m). With a typical accuracy of +/- 3 dB, the sensitivity of a SA depends on the frequency being measured and the range of measurement (Aaronia, 2013). An SA has two detectors: RMS and Min/Max. The Root Mean Square (RMS) is the default detector and can determine the signal power on a given frequency, making it suitable for NIR exposure assessment. Hence the ICNIRP recommends it as mandatory for safety compliance evaluation (Aaronia, 2013). The equipment has a data logger that allows the recording of long-term EMF exposure measurements. The information on the highest reading in each frequency range and matching levels will be continuously recorded when performing SA measurements. All the data recorded can be read by the PC analysis software provided by the manufacturer.

3.3 Analysis Techniques for Electromagnetic Fields

Data analysis combines analytical and statistical techniques to illustrate the data scope, condense its representation, and demonstrate the data through graphs, images, and tables. These processes facilitate the evaluation of statistical inclinations and deduction of meaningful conclusions. The application of statistical techniques coupled with exploratory analysis is vital in informing the status of exposure to NIR.

3.3.1 Statistical Analysis of Electromagnetic Fields

The statistical analysis approach necessitates a good understanding of the raw data, and visual inspection is among the most effective techniques that reveal essential features and trends. The plots used for visualization depend on the type of data set. For instance, a 1-dimensional scatter plot allows data visualization along a straight line and is valid for small data sets that are not too close to each other. The histogram is commonly used to show data trends and allows more explicit recognition of distribution shape (Varmuza and Filzmoser, 2009). The probability distribution function (PDF) comprises a regular line outlining the histogram. Cumulative plots obtained from probability density plots or histograms can also be used to visualize data distribution. The ordinate of the cumulative plot indicates the percentage or number of data values equal to or smaller than the

abscissa value. Cumulative plots are applicable for data with few objects, and normally distributed data exhibits a well-defined S-shape of the cumulative plot.

The descriptive measures of distributions include median, mean, minimum, maximum, and quartiles. Quartiles divide data distribution into four sections corresponding to the 75 percent, 50 percent, and 25 percent percentiles, also referred to as third (Q_3), second (Q_2), and first quartile (Q_1). The 50 percent percentile (Q_2) corresponds to the median value, and the interquartile range is the difference between the third and first quartile ($IQR = Q_3 - Q_1$). The boxplot is an informative graphic that utilizes median and quartiles to summarize the data in a single diagram. The first and third quartiles give the height of the box in a boxplot, while the middle line shows the median value; the box has no significant implication on the distribution. The upper whisker of a boxplot extends from the third quartile to the highest data value in the interval Q_3 to $Q_3+1.5IQR$. The lower whisker extends from the first quartile in the interval Q_1 to the lowest data value $Q_1 - 1.5IQR$ (Varmuza and Filzmoser, 2009). The outliers in a boxplot are found outside the $Q_1 - 1.5IQR$ to $Q_3+1.5IQR$ range and are plotted as individual values. Boxplots help compare distinct data distributions since the boxplots of individual data sets can be displayed side by side.

The central values are essential in describing data sets, and their estimations depend on the data quality. Arithmetic mean is the classical and most frequently used estimator of central value. The average is obtained from the sum of all the elements in a data set divided by the number of values in that set (see equation 3.3). Mean is the most precise estimator of central value for normally distributed data.

$$\bar{x} = \frac{1}{n} \sum_i^n x_i \quad 3.3$$

Where \bar{x} is the mean, x_i the observation, and n is the number of observations in a data set.

The median value provides a robust measure of the central value for a data set with outliers. Median \bar{x}_m divides the data distribution into two equal sets such that the number of data greater than the median is equivalent to the number of elements lower than the median. In cases where the number of data values in a set is even, the arithmetic mean of

the two central values is taken as the median. The extreme values do not affect the median values since it is obtained from the ordering of data values.

The range of data refers to the difference between the minimum and maximum value and is influenced by the outliers that coincide with either minimum or maximum or both. The interquartile range (IQR), which refers to the difference between the first and the third quartile, is a robust counterpart of the range. This value is not affected by up to 25 percent of both extreme ends of the data distribution set. The IQR can be helpful in estimating the theoretical standard deviation of normally distributed data (see equation 3.4).

$$S_{IQR} = 0.7413 \cdot IQR \quad 3.4$$

Where s is the standard deviation and IQR the interquartile range

Standard deviation (s) is the classical and most frequently used measure of data variation and is considerably influenced by the outliers. In cases where data is skewed, the s is more biased than the mean due to the use of squared deviations. Therefore, s is not the appropriate measure of spread in cases of skewed data. Median absolute deviation (MAD) is the robust counterpart of the standard deviation and is based on the median \bar{x}_m as the central value (Varmuza and Filzmoser, 2009). The absolute differences $|x_i - \bar{x}_m|$ are computed, and (MAD) is taken as the median value of these differences. It should be noted that the measures of spread mentioned above assume the same unit as the data values.

Statistical hypothesis testing calls for the conceptualization of the null hypothesis (H_0) that should be tested and the alternative hypothesis H_1 , which describes the alternative. It is important to have a fixed alternative hypothesis, even if they are more than one. The test results comprise the p-value, a probability that assists with the decision. If the p-value exceeds or equals the predefined significance level (5 percent), the test is considered “not significant”; hence, the null hypothesis is not rejected. However, if the p-value is less than the significance level, H_0 is rejected, and it is concluded that the test “is significant” (Varmuza and Filzmoser, 2009). When the significance level is set to be 5 percent, it implies that this fraction of cases in a data set leads to the rejection of the null hypothesis.

The choice of a statistical test requires the type of distribution to be known. In cases where the data distribution is not normal, the results may be misleading, and the use of nonparametric tests offers a solution to such situations since they are less restrictive with reference to the nature of the distribution. Shapiro–Wilk is used for the distribution test to establish whether data is normally distributed or not (Varmuza and Filzmoser, 2009). The null hypothesis for this test indicates that the data distribution follows a normal distribution while the alternative represents the situation in which the data is skewed.

Various methods can be used to test for the central values for making inferences about a data set depending on the type of data distribution. One-Sample t-test requires the data to be normally distributed and samples to be independent. Wilcoxon signed-Rank test is a nonparametric test that requires the data to be continuous and to comprise a symmetric distribution. A two-sample t-test is helpful in comparing the central values for two independent samples. The H_0 of this test implies that the central values of the two samples are equal. It requires the two samples to be independent and have a normal distribution. Wilcoxon Rank Sum Test is a nonparametric test for comparing two central values for independent samples with continuous distributions. The null hypothesis for Wilcoxon Rank Sum Test states that the medians of the two samples are equal.

Visual methods such as histogram can be used to show the data distributions and determine whether it is skewed or not. Python software has useful packages used to perform the data cleaning processes and statistical analysis. This process involves the removal of insignificant values that are below the detection limit. Libraries such as Pandas and Numpy provide useful functions in determining mean, median, absolute deviation, and standard deviations. They can also be used to remove unwanted data values that are below a certain threshold. Subsequently, these libraries can be useful in preprocessing and statistical analysis of EMF data. The Matplotlib and Seaborn libraries are useful tools in Python that facilitate data visualization. These tools were used to determine and visualize different EMF exposure data trends in various locations. Boxplots were used to visualize summarized details of the data such as median, range and quartiles and compare the exposure data of different regions.

3.3.2 Exploratory Data Analysis of Electromagnetic Fields.

Exploratory data analysis (EDA) and visualization tools are used to enhance understanding of the valuable information contained in the data. EDA comprises numerous steps, such as data importation, cleaning, processing, and visualization (Kang, 2013). For instance, data cleaning involves handling noise values, inconsistent data, outliers, and missing values. Some of the approaches used to handle missing data include filling the missing values through regression or mean substitution, average, common-point, or multiple imputations, and carrying forward the last observation (Kang, 2013). Data noise is the deviation in measured values or random errors that result from incidences, such as entry errors and faulty data collection (Alasadi and Bhaya, 2017). Noise can be eliminated using various regression, clustering, and binning methods before transforming it into a suitable form for analysis. Data transformation constitutes the change of structure, format, or values to enhance quality and compatibility between systems and applications.

Dimensionality reduction methods such as principal component analysis (PCA) facilitate the cleaning of data sets, making them easier to analyze and explore. PCA also enables one to extract main components from an existing massive collection of data that provide the most relevant information. Its algorithms are based on variance, covariance, and eigenvalues and vectors. The principal aim of PCA is dimensional reduction; this means to get as much variability (usual variance) as possible with few principal components. Small correlation between variables makes it impossible for dimensionality reduction without losing essential information. The valuable indicator is the PCA score variance usually presented as a percentage of the total variance (Hanson, 2018). If the first two principal components in a score plot preserve more than 70 percent of the total variance, then the scatter plot gives a good representation of the high dimensional data structure.

3.4 Geostatistical Techniques for Mapping RF Measurements

Kriging is a spatial interpolation technique that utilizes a limited set of sampled data points to estimate the variable values over a continuous spatial field. Other methods that can be useful in predicting unknown variables over a continuous space includes Inverse Distance Weighted Interpolation and Linear Regression (Lark *et al.*, 2006). Kriging is different from the aforementioned techniques since it uses the spatial correlation between sampled values to interpolate the values over the spatial field. The kriging interpolation

depends on the spatial arrangement of the experimental observations rather than a postulated model of spatial distribution and produces approximations of the variability surrounding the interpolated values. Kriging can be described as a two-step procedure where the spatial covariance structure of the measured locations is established by fitting a variogram followed by the use of the resulting weights from the covariance structure in interpolating values for unsampled locations across the spatial field.

The weights for every interpolated point are determined based on the spatial structure of the interpolated points in relation to all sampled locations. They are calculated from the variogram depending on the data spatial structure and are linked to the sampled locations according to the expression 3.5 (Ali *et al.*, 2006).

$$\hat{z}(x_0) = \sum_{i=1}^N \lambda_i Z(x_i) \quad 3.5$$

In equation 3.5 above, the value of the estimated point (\hat{z} , at location x_0) is equal to the summation of the value of every sampled location (x at point i) multiplied by that location's distinct weight (λ for point i). The covariance matrix from the approximated variogram is utilized in determining the weights.

Generally, the weights in kriging are determined such that points close to the region of interest are accorded greater weight than others at far distances. Points clustering is also taken into account so that the cluster of points are weighted less heavily (practically, they have less information than a single point). Subsequently, there is minimized bias in the predictions (Lark *et al.*, 2006). The predictor in kriging is an “optimal linear estimator” and an exact interpolator, implying that every interpolated value is calculated to decrease the estimation error for that point. The values generated by the kriging process for a particular point is equal to the empirical values at that point and all the interpolated values are the Best Linear Unbiased Predictors (BLUPs) (Lark *et al.*, 2006). Kriging is an effective interpolation technique due to its ability to preserve the spatial variability that is likely to be lost when using other methods.

A variogram is a visual representation of the covariance between each pair of points in the collected data (see equation 3.6). The gamma value or “semi-variance” (the measure of half mean-squared variation between their values) for every pair of points in the collected

data is plotted against the lag (distance) between them (Ali *et al.*, 2006). The experimental variogram comprises the plot of measured values, while the model (theoretical) variogram has the distributional representation that best fits the data.

$$\hat{\gamma}(h) = \frac{1}{2m(h)} \sum_{i=1}^{m(h)} [z(x_i) - z(x_i + h)]^2 \quad 3.6$$

Where $\hat{\gamma}(h)$ is the approximated semi-variance for the interval h and $m(h)$ is the value of determined point pairs in the vector space class h . $Z(x_i)$ is the estimator at point x . The empirical variogram is a function between direction and distance and is relatively easier to calculate when the field has isotropy. Anisotropic spatial trends necessitate the extraction of various variograms in the typical sets of directions (Mohebzadeh, 2018). Two major assumptions (isotropy and stationarity) are made for kriging to offer the best linear unbiased estimation (Abzalov, 2016). However, some kriging methods allows the strictest form of the assumptions to be altered. The stationarity assumption implies that the joint probability distribution remains unchanged across the study area; parameters (overall values mean, the sill, and range of the variogram) remain constant. The same semi-variogram model is considered to be valid across the study region. The isotropy implies uniformity in all directions.

The experimental variogram estimators do not always meet the statistical requirements of a variogram despite being essential tools for scrutinizing spatial correlation. Therefore, these models cannot be utilized in spatial prediction or regression since they do not certainly signify a rational spatial process. Subsequently, a theoretical curve with a defined mathematical formula (theoretical variogram) is used to define the experimental variogram curve. Typically, models such as circular, spherical, Gaussian and Exponential variograms are used to fit a theoretical model to the experimental variogram (Mohebzadeh, 2018). Visual inspection is the most common approach in determining the best variogram fit. In this case, an individual plots the empirical model and then tries to identify a linear combination of theoretical variograms, which yields a graph that is similar to the experimental one. The main disadvantage is that this method lacks statistical justification and different individuals can fit distinct theoretical models to the same empirical variogram. However, a plot of the experimental curve can help one identify problems with the data and the calculations.

3.5 Assessing the Electric Field Exposure for ICNIRP Compliance

All signals in an environment with multiple frequencies contribute to personal exposure since their impacts are additive. Therefore, the total exposure can be demonstrated in terms of exposure quotient based on the measured electric field of every signal and the reference level provided by the ICNIRP corresponding to that particular signal frequency (Lahham and Hammash, 2012). Equation 3.7 shows the expression used to obtain the exposure quotient for the various radiofrequency signals. The location with the highest total electric field can be identified and parameters such as exposure quotient, total exposure quotient, and times below limit calculated to establish whether the exposure to EMF is compliant with the ICNIRP guidelines.

$$\text{Exposure quotient} = \frac{E}{E_{ref}} \quad (3.7)$$

Where the E is the measured electromagnetic field corresponding to the frequency of the signal and the E_{ref} is the electric field reference level provided by the ICNIRP guidelines corresponding to the frequency of that signal. The E_{ref} value can be determined from the expression shown in Table 1.1. The total exposure quotient can then be expressed by equation 3.8.

$$\text{Total exposure quotient} = \sum_{i=1}^{N_t} \frac{E_i^2}{E_{ref}^2} \quad (3.8)$$

Where N_t is the total number of signals contributing to the exposure, E_i is the measured electric field corresponding to the signal frequency and E_{ref} is the electric field reference level provided by the ICNIRP guidelines. The factor for estimating the number of times the exposure level is below the safe limits (Times below limit (TBL)) can be obtained from equation 3.9 below.

$$TBL = \frac{1}{\sum_{i=1}^{N_t} \frac{E_i^2}{E_{ref}^2}} \quad (3.9)$$

CHAPTER FOUR

METHODOLOGY

4.1 Chapter Overview

This chapter aims to provide a discussion of the measuring equipment and methods used during the study. An overview of the most appropriate regions and factors considered for the RF-EMF study is given and procedures employed during data collection and analysis. Lastly, a description of how the heatmaps were used to show the variation of electric field strength is provided.

4.2 Measurement of RF-EMF Exposure Levels

During the measurement of electric field, a frequency-selective spectrum analyzer was used. Different regions where the measurements were performed are described below. The parameters considered during the measurements have been described in the sections below.

4.2.1 Aaronia Spectran HF-6065 Used for Measurements of Electric Field

The Aaronia Spectran HF-6065 was used to measure radio frequency signals within selected frequency ranges in this work (see Table 4.1). The equipment can measure frequencies ranging from 10 MHz to 6 GHz and was connected to a directional HyperLOG antenna with a frequency range of 700 MHz to 6GHz by a 1m SMA cable. The spectrum analyzer was set to measure the electric field strength of the signals associated with the downlink frequency bands considered for this study during EMF data collection. The default setting of the RMS detector was used when collecting electromagnetic exposure data as recommended by the ICNIRP (Aaronia.com, 2005-2013). The SA had insufficient memory to store large quantities of EMF data and therefore was connected to a PC that stored data using a USB cable as shown in Fig. 4.1. Besides, the MCS software installed on the computer to facilitate data collection allowed for real-time visualization of signal strengths and their associated frequencies as the data was continuously loaded.

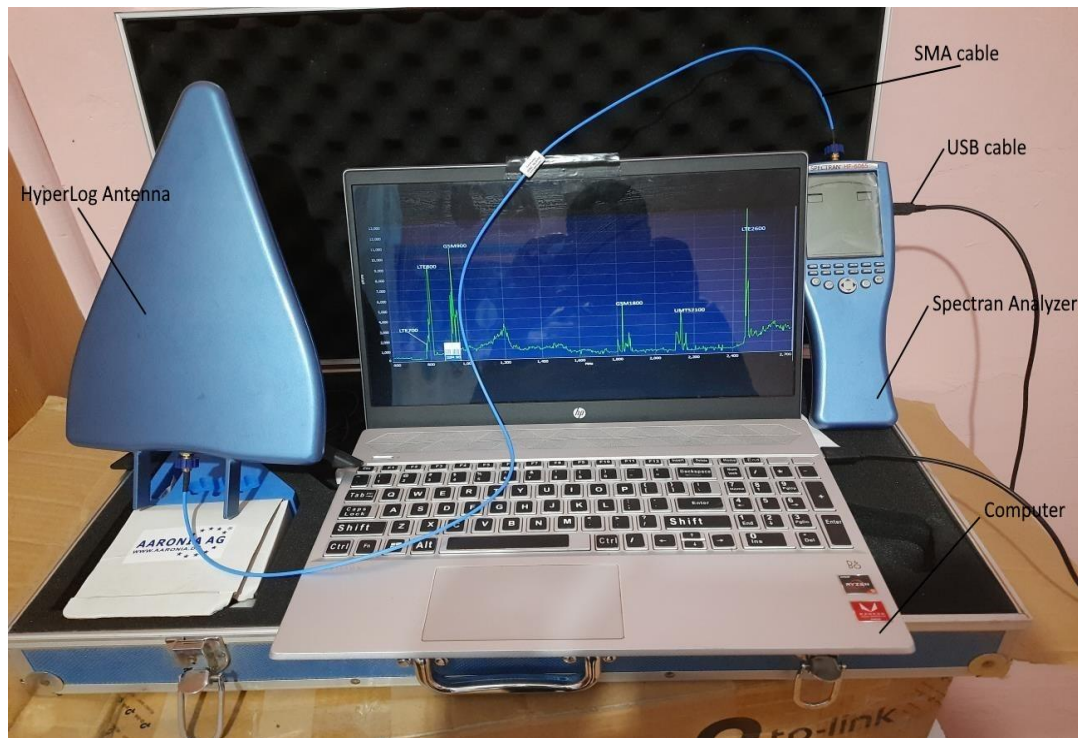


Fig. 4.1: Spectrum Analyzer connected to a PC.

4.2.2 Parameters Considered in the RF-EMF Measurements

Although electromagnetic fields are a combination of both magnetic and electric fields, the latter is the main component affecting biological tissues (ICNIRP, 2020); thus, the focus of the present work. Table 4.1 shows the telecommunication services operating frequencies used as a guide in setting the SA during the measurements. Both geographical position and electric field information about data collection locations were recorded with the help of MCS software and stored on a personal computer. The equipment was set to take samples of electric field strength in intervals of 500 milliseconds. The direction with the strongest signals was identified by observing the signal strength on the computer while slowly rotating the HyperLOG antenna in different directions. Once the direction with the strongest signals was identified the electric field values were collected by holding the Hyperlog antenna at arm's length at approximately 1.5 m from the ground. The electric field value per location was obtained from averaging the recorded instances in approximately six minutes, which accounts for the mean time required for the thermoregulatory mechanism of body tissues to retain equilibrium (ICNIRP, 2020).

Table 4.1: Cellular phones operating frequency bands (Source: CAK, 2018).

Band	Uplink (MHz)	Downlink (MHz)	Band Name
1	1920 – 1980	2110 – 2170	UMTS 2100
2	1710 – 1785	1805 – 1880	GSM 1800
3	880 – 915	925 – 960	GSM 900
4	703 – 733	758 – 788	LTE 700
5	791 – 821	832 – 862	LTE 800
6	2500-2570	2620-2690	LTE2600

4.2.3 Sites Considered for the RF-EMF Exposure Survey

Nairobi City is the headquarters for most telecommunication services providers, various governmental and non-governmental institutions, multiple business activities, and multi-dwelling residences; hence, it was the most appropriate region for Kenya's preliminary NIR assessment study. Nairobi city has a population of 4,397,073 as reported by KNBS census in 2019. The geographical coordinates of the city are 1° 17' 0" South, 36° 49' 0" East. Furthermore, there are numerous radiofrequencies transmitting structures in the area, including television and FM broadcasting, mobile telephony base transceiver stations, and emergency service communication networks. For instance, the results from this study would also give a representation of NIR exposure status in most developing countries. The considered sites for the survey are populous and therefore numerous BTS are erected to meet the network demand for the residents. The distance from the source of RF-EMF is a primary factor that was considered during the measurements since several studies have shown that the severity of radiofrequency effects on health depends on the distance between the sources and the dwelling places (Enyinna and Avwir, 2010; Santini *et al.*, 2002). Table 4.2 gives a brief description of the various sites that were earmarked for NIR assessment.

Table 4.2: Description of Identified Sites for NIR assessment

Site	Description
1. Site 1 (residential area)	Measurements were obtained from a school playground in Umoja I area Four measurements were obtained in two separate 2-storey buildings in Umoja II and Umoja III.
2 Site 2 (residential area)	Two measurements were obtained from an open field (Near a school playground and the premises of a recreational facility) in Ngong town.
3 Site 3 (residential area)	RF-EMF measurements were done at every floor 4-storey in building in Zimmerman.
4 Nairobi CBD	The RF-EMF data was collected from 51 points in the Nairobi Commercial Business District.

Electromagnetic radiation exposure levels from RF-EMF fields were assessed from selected sites within commercial and residential areas in Nairobi and its environs. Nairobi CBD was chosen to represent the commercial areas. Residential areas comprised residential buildings, schools, businesses, and hospitals. In the residential areas, the choice of RF-EMF data collection points was informed by environmental setting of the chosen areas (i.e., proximity of BTS to residential buildings, schools, and hospitals) informed the most suitable data collection points. Data was sampled in open fields and within buildings in the residential areas.

The RF-EMF data in site one was measured in AIC school playground in Umoja 1. At the time of measurements, the school had pupils up to grade four and was approximately 30 m from a BTS surrounded by several antennas at different heights. The RF-EMF exposure data in another site were collected on a 4-floor residential building neighboring a base station erected at the rooftop of another building. The data was collected on the balconies of two floors in the residential building (first and second) since the other floors were not accessible. The data collection in the third site was performed on two floors of a building near Mama Lucy Kibaki hospital and approximately 50 m away from a BTS that had several antennas fixed at different heights. The ground floor was not accessible, and therefore the data was collected on the stairs of the first and second floors.

The RF-EMF measurements in fourth and fifth sites were performed at two points: near Edmund Rice Catholic Education Center entrance and a shopping center near the school. The institution near the measuring point was approximately 200 m from the BTS that had several antennas surrounding the mast at different heights. The other RF-EMF data collection point was near a shopping center in Ngong and was approximately 100 m away from a BTS. The RF-EMF exposure data in other measuring sites were collected on each of the four floors of a residential building whose rooftop is used for basking and drying clothes. The building was surrounded by other residential facilities and had antennas for various service providers at every rooftop corner.

The behavior of electric fields propagation in different directions was assessed from a base station surrounded by residential buildings in Ruiru. A BTS neighboring residential houses and other social amenities (approximately 20 m radius) was identified, and several measurements of electric field performed at intervals of 30 m towards the three directions. Five measurements were performed towards the three different directions. The measurements obtained were used to investigate how direction and distance from the BTS affect the intensity of electric field.

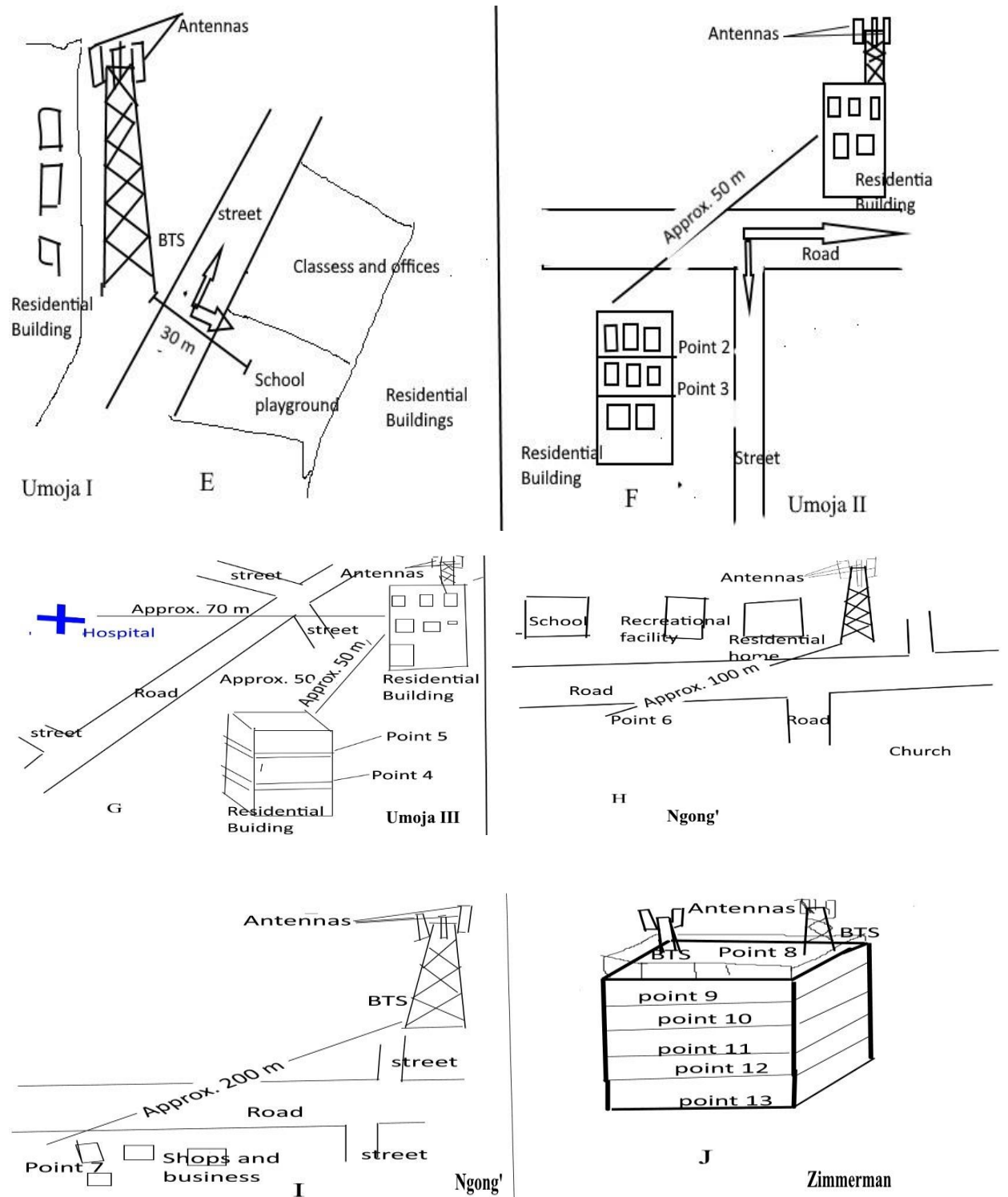


Fig. 4.2: Illustration of EMF measurement points in residential areas.

The environment in CBD was rather complex in relation to the assessment of electromagnetic exposure levels. This is because BTSs are usually fixed at the rooftops and walls of various buildings and some of them may not be easily located. Practically all

locations further from one base station can be closer to another base station, and it becomes challenging to accurately state "how far" one is from a radiating antenna. Therefore, the data collection approach in Nairobi CBD was different from the residential areas. A grid with intervals of 200 m was made, and measurements were carried out at the grid intersection points that were marked on Google Maps before the actual measurements were done. During the measurements, the predetermined points of EMF data collection on Google Maps were located with the help of the Global Positioning System (GPS) of a smartphone device. Where the marked coordinates were inaccessible due to factors such as buildings and other physical structures, the measurements were performed as close to the point as possible. Fig. 4.3 shows a Google Map of Nairobi CBD with the data collection points labelled from 1 to 51.



Fig. 4.3: Nairobi CBD map with labelled points where EMF measurements were done (Source: Google Maps).

4.3 Analysis of the RF-EMF Exposure Measurements.

After the data collection, statistical and exploratory data analysis was performed in order to enhance the understanding of exposure to electric fields. The safety status was established by comparing the results with ICNIRP guidelines.

The exposure levels associated with various frequency bands were determined from the quadratic sum of individual frequencies within that band while the total electric field exposure (E_T) was calculated by summing up all the electric field values of the frequency bands. Only the downlink frequency was considered for this study since it comprises signals transmitted from the BTS to the mobile phones (Saravanamuttu *et al.*, 2015). The raw data collected needed to be processed and analyzed to gain insights into the patterns and trends of RF-EMF exposure in Nairobi city and its environs. A typical spectrum of RF-EMF comprises several peaks of varying heights. The intervals between the peaks represent the frequency regions that are not utilized for telecommunication purposes and hence include the noise from the measuring equipment. This data was discarded since it carried no vital information regarding this study. A preliminary investigation of useful data was performed to see the most appropriate measure of central tendency describing the exposure. Comparing the mean and median of the data was one of the methods used to check whether the data followed a normal distribution or not.

The data analysis of EMF exposure level was imported into the R program as a single file with data grouped into commercial and residential using the *matrix2SpectraObject* function. The file had 26 data columns (13 columns for each category). There were 13 measurement samples from the residential areas. For the purpose of PCA analysis, 13 measurement samples of electric field were systematically picked based on the position of the sampling point geographical coordinates on the CBD map. These points (1, 3, 5, 7, 24, 22, 20, 18, 33, 35, 37, 39, 50) are indicated on Fig. 4.3. Each column in the file had several rows with electric field strength values corresponding to frequencies of various relevant bands. The imported data were summarized with the help of the *sumspectra* algorithm in *Chemospec* to and the results used to confirm whether the data had the appropriate features. This function also allows for verification of the data range and whether it meets expectations.

The entire set of EMF spectra was inspected to establish regions with no significant information using the *SurveySpectra* function. This algorithm calculated the summary

statistics of the electric field intensities at different frequencies across the data set. The upper/lower and the mean/median lines were plotted closer together for regions with little variations. The `check4Gaps` function was used to show the empty regions with the spectra. The `c_pcaSpectra` algorithm was used to perform classical PCA analysis and the scores of the results were plotted using the `plotScores` function. The s-plot helps determine the variables with the most significant influence on the variation of the data. The function `sPlotSpectra` plots the correlation of each frequency variable with a given score against the covariance of that frequency variable with the same score. This function produces an s-shaped plot with the most dominant frequency variables in the lower left and top right quadrants (Hanson, 2018). It was used to show the individual frequencies with different bands that contributed to the most significant exposure variation of RF-EMF exposure.

The R programming language comprises packages that offer all the necessary functions in processing and analyzing the data (R Core Team, 2021). For instance, *ChemoSpec* is a group of functions R that are useful in top-down exploratory data analysis of spectral data such as nuclear magnetic resonance, infrared (IR), and other similar types of spectroscopy. It has functions for peak alignment, principal component analysis (PCA), plotting and inspecting spectra, hierarchical cluster analysis (HAC), and model-based clustering. *ChemoSpec* is made to accommodate samples with distinct histories, i.e., different categories or groups. As shown in Fig. 5.1 the peaks in the diagram span few frequency units, top-up and shift back to the baseline. Any point in a given peak describes much of the same thing, i.e., the electric field intensity. Also, frequencies for every peak rise and fall simultaneously as the peak changes from one sample to another.

Two functions can load the data into the *ChemoSpec* for analysis: `files2SpectraObject` and `matrix2SpectraObject`. The former assumes that the data comprises separate files in a particular directory with intensity and frequency columns. The data can be separated by characters such as tab space, semicolon, comma, etc., and it's not a must for the header row to be present. The `matrix2SpectraObject` function assumes that there is a single data file containing a matrix of the data. The first column of this file should have frequencies, and the others comprise individual sample intensities. This function requires the data to have the header row with sample names. The output of the two methods mentioned above gives a spectra object with the data and other associated information that R-program can interpret.

Various options can be utilized in the principal component analysis as outlined by (Hanson, 2018). The main options for performing PCA in *Chemospec* are robust and classical methods. The classical techniques use all the data provided to compute the loadings and scores. The main focus of robust methods is the core of the data, and hence some data is outweighed. Although the two techniques attempt to get the PCs that explain most of the data variation within a given data set, their results differ significantly. *plotScore* function can be used to generate a 2D plot of the classical PCA results.

4.4 Spatial Interpolation of the RF-EMF Measurements

Geospatial mapping was performed for the data collected for each data collection point in Nairobi CBD. The total electric field values, obtained from the quadratic sum of all the downlink frequencies was used to make electric field exposure maps. The results were used to design a map that facilitated visualization the spatial distribution of RF-EMF measurements across the sites on a two-dimensional grid. In general, this geospatial mapping may be used to show response variation as a function of two covariances variegating in a grid-like pattern, such as electric field strength as a function of distance from the source or the number of sources. Every grid point in these maps is related to a polygon, and individual polygons are colored using a color scheme associated with the response at each point in the grid (Abzalov, 2016). The image is often accompanied by a color scale associating the colors to the levels of response.

The *sp package* embedded in the R program offers powerful classes for displaying geographically referenced data. The *splot package* and *ggplot2 package* were used to generate heat maps for the spatial gridded data frame class objects as reported by French (2017). Functions in the *sp package* were also used to handle geographic data to enhance interoperability between various analysis packages that utilize spatial data. The basic structure for spatial objects (i.e., line, polygon, point) in the *sp package* is appropriate to describe the Coordinate Reference System. The *ggmap* package helps one download various base maps, including satellite imagery, to integrate them with *ggplot* package in R, which plays an excellent role in making graphs and facilitates the visualization of spatialized data. The mapping of the data comprised the generation of interpolation grid, and the gridded prediction was performed using kriging.

The mapping process started with loading the data that comprised geographical coordinates and total electric field values in different columns of a csv file into R. The total electric field data was spatialized with the help of the *ggmap* function, which is also useful in downloading different types of base maps such as satellite imagery. After downloading the Google satellite map, the electric field exposure data was overlaid based on longitude and latitude attributes. The geographical coordinates in the data were used to compute the area of interest for which the spatial interpolation was performed. A grid with a 25-meter resolution was generated using the *GridTopology* function in R. Spatial points with the same coordinate system as the boundary of the grid was generated using the *SpatialPoints* function. The crop algorithm in R was used to crop out the region of interest. The values to predict, data set, output data, variogram model were passed to the kriging function and predictions over the grid was performed.

CHAPTER FIVE

RESULTS AND DISCUSSION

5.1 Chapter Overview

This chapter aims to provide the results obtained from the study. It comprises the measurements results, analysis and comparison of the results with the ICNIRP guidelines to establish whether exposure is within the acceptable limits. The explanation for various data trends observed in the results is also explained. Lastly, the EMF in Nairobi CBD data mapping is also discussed in details.

5.2 Results of RF-EMF Exposure Measurements

The sections of the electromagnetic spectrum used for signal transmission as shown in Fig. 5.1 have corresponding high values of electric fields. The bands involved with radiofrequency transmission are shown in Table 4.1. It was found that the highest peak in the spectrum varied from one measurement point to another. Measurement results showed that the strength of signals for different bands varied from one measurement point to another.

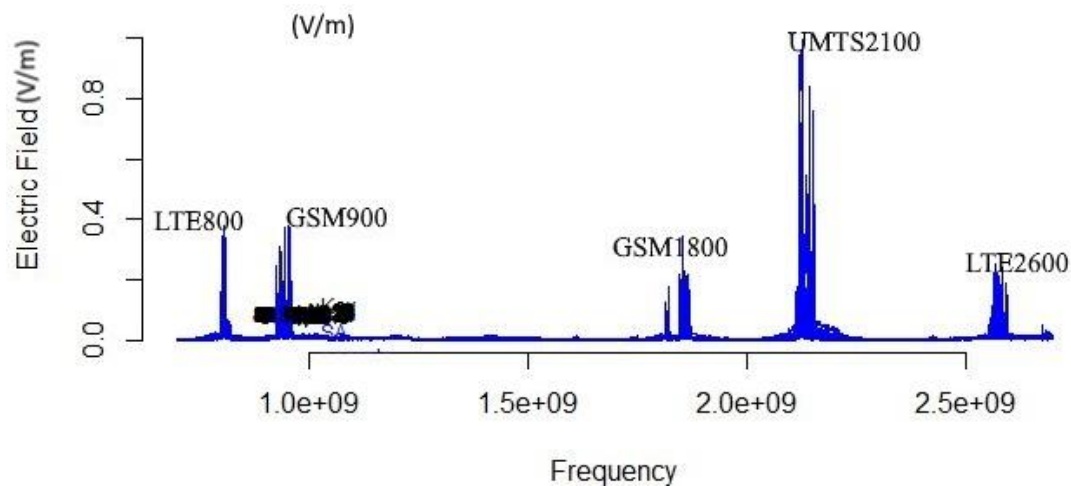


Fig. 5.1: Typical spectrum showing various bands used for telecommunication services.

It was also observed that some signals were not detected at locations; for instance, the LTE 700 signals were not detected at Zimmerman residential building. This observation implies that there was no transmitting antenna operating at frequencies of LTE 700 at the points where measurements were taken.

From the measurements performed, it was observed that the exposure to electric fields varied considerably from one point to another. It was also evident that the electric field values kept on fluctuating throughout the time of measurement. For instance, Fig. 5.2 shows a graphical representation of electric field measurement variations for measurements obtained from one point. The frequency bands considered for this study exhibited distinct magnitudes of electric fields at different measurement points. It was also observed that the values of the electric field from the same BTS but different directions varied significantly.

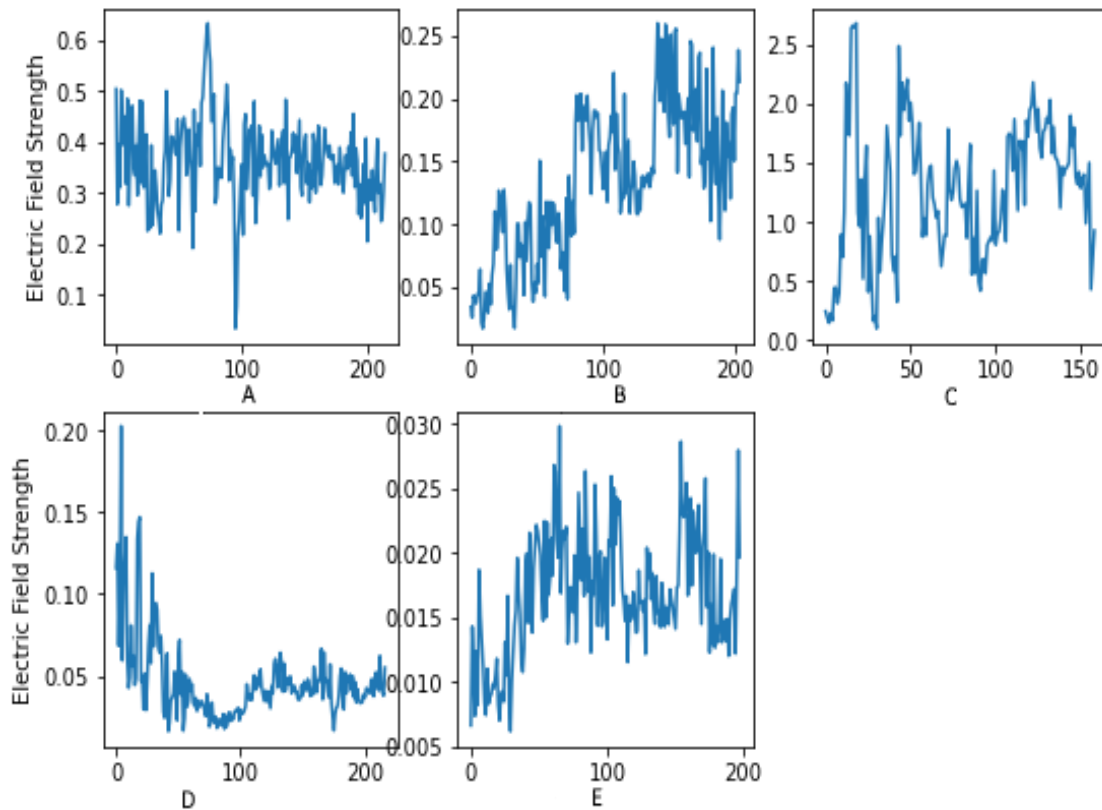


Fig. 5.2: The electric field variations for various frequencies at the time of sampling.

As reported in previously (see section 3.1), the intensity of electric field radiated by directional transmitting antennas is high within the main lobe and reduces as the distance from the center of the propagation path increases. The electric field strength reduced as the distance from the source (BTS) increased due to space loss (Salous *et al.*, 2020). The values of electric field at the same distance from the BTS but different directions showed significantly different values since most of the BTS have directional antenna that transmit

signals in a particular direction. The values of electric fields were higher in the directions where the antennas faced which is the main lobe of the transmitters. It was also observed that the electric field values measured at the base of the BTS were lower than distant measurements (≈ 50 m). The transmitter antenna is designed to transmit signals over a wide space. Therefore, the antenna is designed to face away from the BTS and inclined towards the ground. The region where the emitted signals hit the ground experiences the highest electric field intensity. The variations in the values of electric field as one changes the direction and distance from the antenna was expected due to the inherent characteristics of electric fields as discussed in the previous chapters.

The electric field data collected for every band comprised several peaks of different heights and empty regions shown in Fig. 5.1. To identify the insignificant measurements for this study, the equipment was used to take electric field measurements of an enclosed room without connecting its antenna. The results were used to inform the minimum value acceptable to represent the measure of the electric field after connecting the probe. All the measurements below 0.005V/m were considered insignificant for this study and therefore discarded. A preliminary investigation of the data (mean and median values of data samples) collected in every location also showed that the samples were not normally distributed. It is important to consider the nature of data distribution when choosing the measure of central tendency to use for its description. The mean (average) is commonly used to describe data but it is not ideal for data with extreme values or outliers. However, the median is not affected by the extreme values of a skewed data distribution since it utilizes the value at the middle of ordered data set. Thus, the median was considered the most appropriate to describe the data.

5.2.1 RF-EMF Levels in Residential Areas

The residential areas measurements were analyzed separately and then compared with the Nairobi CBD region. Table 5.1 shows the summary of electric field measurements obtained from various data collection site for different bands in residential areas.

From the results, it can be shown that the exposure within the same building varies from one floor to another, see sites: 1 and 3 in Table 5.1. In site 2, the total electric field values were 0.613 V/m and 0.391 V/m . From the summary of the results, it was found that

different points had distinct exposure levels. It was found that the highest values of total exposure were recorded on the higher floors of buildings in three measurement sites. This observation can be attributed to obstacles between the floors and transmitting antennas. Another factor contributing to this observation can be the point of measurements being closer to the path of propagation of the transmitted signals. In all the places, the transmitting antennas were within a radius of 300 m from the point of measurements.

Table 5.1: Summary statistics of different residential areas.

Sites	Mean	Std	Min	Q1	Median	Mad	Q3	Max
1	0.909	0.285	0.567	0.748	0.940	0.191	0.961	1.331
2	0.502	0.157	0.391	0.447	0.502	0.111	0.558	0.613
3	1.055	0.682	0.451	0.556	0.916	0.414	1.229	2.279

5.2.2: RF-EMF Levels in the CBD

The summary of the results in Table 5.2 shows that the median and mean values (0.9011 and 1.146V/m) for the electric field exposure in the Nairobi CBD region were different. This difference suggested that the data was skewed, and the Shapiro test of normality was used to confirm the nature of the distribution. The results showed that the exposure data in CBD region was not normally distributed ($W = 0.84702$, $p\text{-value} = 1.085e-05$). Although mean and median values can be used to describe the central tendency of a data set, the former is considerably susceptible to outliers' influence (Varmuza and Filzmoser, 2009). The mode, median, and mean are identical for normal distribution and represent the most typical value in a given data set. However, skewing in a data set makes the mean lose its ability to represent the most appropriate measure of central tendency since such data tends to drag it away from the typical value.

Table 5.2: Descriptive statistics for the total electric field in the CBD region.

	Mean	Std	Min	Q1	Median	MAD	Q3	Max
Totals Electric								
Field (V/m)	1.146	0.7826	0.1392	0.6530	0.9011	0.3037	1.291	3.667

On the other hand, the median value divides the number of observations in a data set into two groups based on order, takes the middle value, and is hence not affected by the skewed values. The EMF exposure data Nairobi CBD was skewed to the left, as shown in Fig. 5.4. Therefore, the median value was the most appropriate value to describe the exposure. The median value of electric field exposure in the CBD region was 0.901 V/m while the Q1 and Q3 were 0.653 and 1.291 V/m, respectively. The minimum value of electric field exposure was 0.139 V/m, and the maximum value was 3.667 V/m. This indicates that the exposure to RF-EMF in CBD different sites experience distinct exposure to electric fields since the highest exposure was 26 times higher than the lowest exposure value.

5.3 Results of Variability Assessment of RF-EMF Levels and Comparison with ICNIRP Values

The analysis of the electric field data obtained showed different features of the data. For instance, the statistical analysis revealed the magnitudes of electric field at different measurement points while the exploratory analysis enhanced the understanding of different aspects of variations in the electric field intensities in the residential and commercial regions.

The results of the measurements in all the sites showed similar characteristics with the previous studies in different places. From previous chapters, it was reported that the intensity of the electromagnetic field depends on the position of measurement relative to the source. The sector antennas used for telecommunication signal transmission radiate more energy in the intended horizontal direction of radiation (Staebler, 2017). Therefore, the intensity of RF-EMF is likely to be higher within the main lobe (intended direction) and reduces as one moves away from the center of the propagation path. Another aspect of transmitting antennas likely to contribute to the observed variation is vertical directionality. The telecommunication antennas transmit power with a reasonably narrow beam that is normally tilted slightly downwards depending on the height of the mast and the region of coverage. Subsequently, the measurement points that were within the RF-EMF transmission paths experience higher exposure than others.

The variations in electromagnetic field levels of the building in site 3 as shown in Fig. 5.3 can be attributed to varying distances between the main lobe of radiating antennas and the points of measurements. As one moves from the rooftop towards the lower floors, the far they are from the propagation paths. Similarly, the exposure to electric fields decreases with increasing distance from the rooftop. Reflections and attenuations of electromagnetic waves by walls of the building are also likely to interfere with the propagation of the electromagnetic waves causing reducing electric field intensity. It is important to note that the contributors of exposure can also result from antenna from different places.

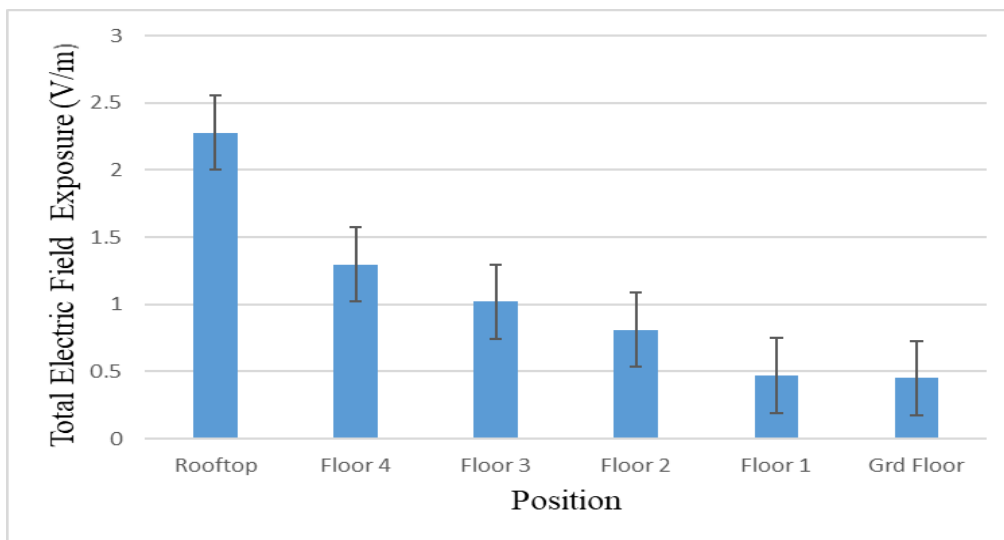


Fig. 5.3: Variation of the total electric field in a residential building in site 3

The median values of total electric field exposure in the three residential sites considered during the study were 0.94 ± 0.19 , 0.502 ± 0.11 , and 0.916 ± 0.41 V/m, respectively (see Table 5.2). It is evident that exposure in the areas differed significantly despite all of them being collected from points near base stations. Such occurrence can be attributed to various factors including the point of measurement relative to the vertical symmetry of the radiating antenna; measurements within the main lobe are expected to be higher than the side lobes. Besides, the traffic on a given BTS influences the intensity of electric field (Staebler, 2017). In the present study, site one had the highest value, while site two had the least total median exposure value.

The signals transmitted by the radiating antennas are influenced by the number of connected devices. Generally, site two (Ngong town) is not as populous as site one (Umoja); therefore, the network traffic from the radiating antennas in the two places is likely to differ. Besides, the measurements in the two regions were performed at places with distinct set ups which increases the possibility of electric field intensity variations. Some data collection points were considerably closer to the BTS and at different heights. Consequently, measurements collected more closer to the main propagation paths (main lobe) of electromagnetic fields contributed to higher electric field values in site one than in site two. All the measurements in site two were performed on the ground and identifying the points where the main lobe hits the ground was complex since the areas surrounding the BTS were not accessible to the public.

The frequency bands (see Table 4.1) measured in the residential areas were explored to get more information about how they influence exposure to electromagnetic fields. From Table 5.3, it can be shown that multiple frequency bands contributed differently to the exposure. GSM900 was the highest contributor to the electric field exposure (30.3 percent), while LTE700, which was not detected in Site 3 contributed the least (3.4 percent) in residential areas. The median value of the GSM900 was 0.499 V/m, while that of LTE700 was 0.056V/m. The highest value of GSM900 was 1.195 V/m which was measured on the balcony of the second floor in site two and contributed 51.04 per cent of the exposure at that point. Both LTE2600 and LTE700 contributed to less than 10 per cent of the electric field exposure in the residential areas. The highest value of UMTS2100 was 1.873 V/m measured at the rooftop of a residential building in site three.

Table 5.3: Summary of the frequency bands in the residential areas.

	Mean	Std	Min	Q1	Median	MAD	Q3	Max	%
LTE700	0.031	0.049	0.000	0.000	0.056	0.036	0.056	0.165	3.4
LTE800	0.337	0.161	0.083	0.255	0.307	0.146	0.462	0.620	18.6
GSM900	0.525	0.268	0.123	0.353	0.499	0.146	0.607	1.195	30.3
GSM1800	0.321	0.176	0.000	0.261	0.312	0.125	0.437	0.611	18.9
UMTS2100	0.460	0.454	0.117	0.266	0.333	0.144	0.477	1.873	20.2
LTE2600	0.175	0.180	0.000	0.072	0.140	0.084	0.224	0.665	8.5

Although the maximum electric field value per band resulted from UMTS2100, the highest median exposure value was associated with GSM900 (see Table 5.3). It is also evident that some bands, such as LTE700 and GSM1800, had minimal contributions to RF-EMF exposure in some places, as shown in the Table 5.3. The median values of electric field exposure associated with LTE700 and LTE1800 were 0.056 and 0.312 V/m, respectively. The LTE800 band contributed 18.6 per cent of the exposure, and its median value was 0.307 V/m. UMTS2100 was the second highest contributor of exposure to electric field (20.2 percent), while the GSM 1800 and LTE2600 bands contributed to 18.9 and 8.5 per cent, respectively. The median values for the frequency bands were used to plot the boxplot. It was found that the LTE700 band had the lowest range of exposure values compared to the other bands. The interquartile range of the GSM900 band was significantly greater than the other bands.

The variation to the EMF exposure in the CBD can be attributed to the set-up of the area since the radiofrequency emitting antennas in the CBD are mostly fixed on the walls of the buildings. Since, the electromagnetic waves are attenuated by physical structures such as walls of buildings, the levels of electric field exposure are likely to be considerably low where there are barriers between the point of measurement and radiation source.

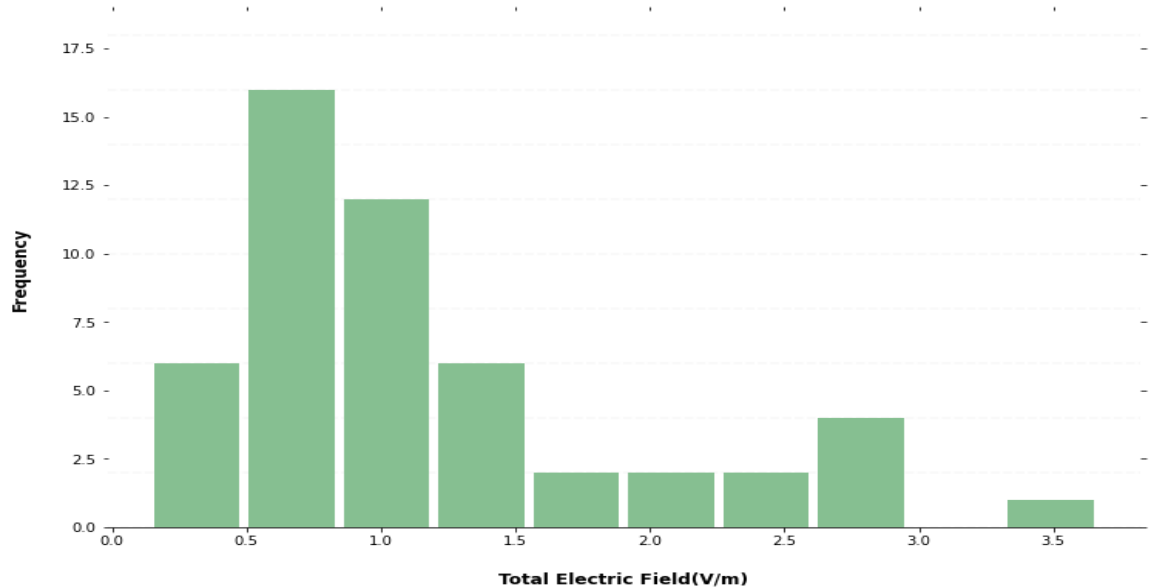


Fig. 5.4. Histogram of electromagnetic field distribution in CBD region

Assessment of the measurements performed in this study showed that different frequency bands contributed differently to the electromagnetic fields exposure just like in the

residential areas. Table 5.4 shows the summary of various frequency bands in Nairobi CBD. The percentage of contribution to exposure by individual frequency bands varied considerably. From summary table 5.4, it can be shown that GSM900 contributed 46.42 per cent of the exposure in CBD while LTE700 contributed 3 percent. The other frequency band contributing less than 10 per cent of the total exposure was LTE2600 (5.85 percent). UMTS2100 and LTE800 contributed 12.98 % and 12.9 % of the exposure. The highest electric field value came from UMTS2100, but its median value (0.1762 V/m) was lower than GSM900 (0.6304 V/m). GSM1800 was the second-highest contributor to the electric field and had a median value of 0.256V/m.

Table 5.4: Electromagnetic field for various bands in Nairobi CBD

Band	Mean	Std	Min	Q1	Median	MAD	Q3	Max	percent
GSM1800	0.402	0.425	0.002	0.134	0.256	0.168	0.528	2.075	18.8
GSM900	0.766	0.596	0.012	0.426	0.630	0.244	0.912	2.720	46.4
UMTS2100	0.397	0.625	0.045	0.125	0.176	0.084	0.347	3.375	12.9
LTE700	0.060	0.051	0.016	0.032	0.041	0.014	0.061	0.289	3.1
LTE800	0.201	0.128	0.006	0.127	0.175	0.064	0.248	0.700	12.9
LTE2600	0.133	0.140	0.033	0.059	0.079	0.031	0.135	0.713	5.9

It was found that the range of GSM900 exposure had the greatest interquartile range while LTE700 and LTE2600 had the lowest interquartile ranges and median exposure values. It was also evident that the median values of the various frequency bands were different. The exposure levels from different RF sources vary from one point to another depending on factors such as distance from the transmitting antenna, structures, and the power output of the transmitting antennas, among others. Fig. 5.5 shows a graphical representation of how electric field exposure varied for different points in Nairobi CBD. From the diagram, point 34 had the highest electric field exposure value while point 18 had the lowest value. An antenna was shown hanging at a height of approximately three meters above the ground on the wall of a building that was approximately 20 m away from site 34. On the other hand, measurement at point 18 were made along a street between high-rise buildings. All directions were visually inspected and no antenna was found close to the point.

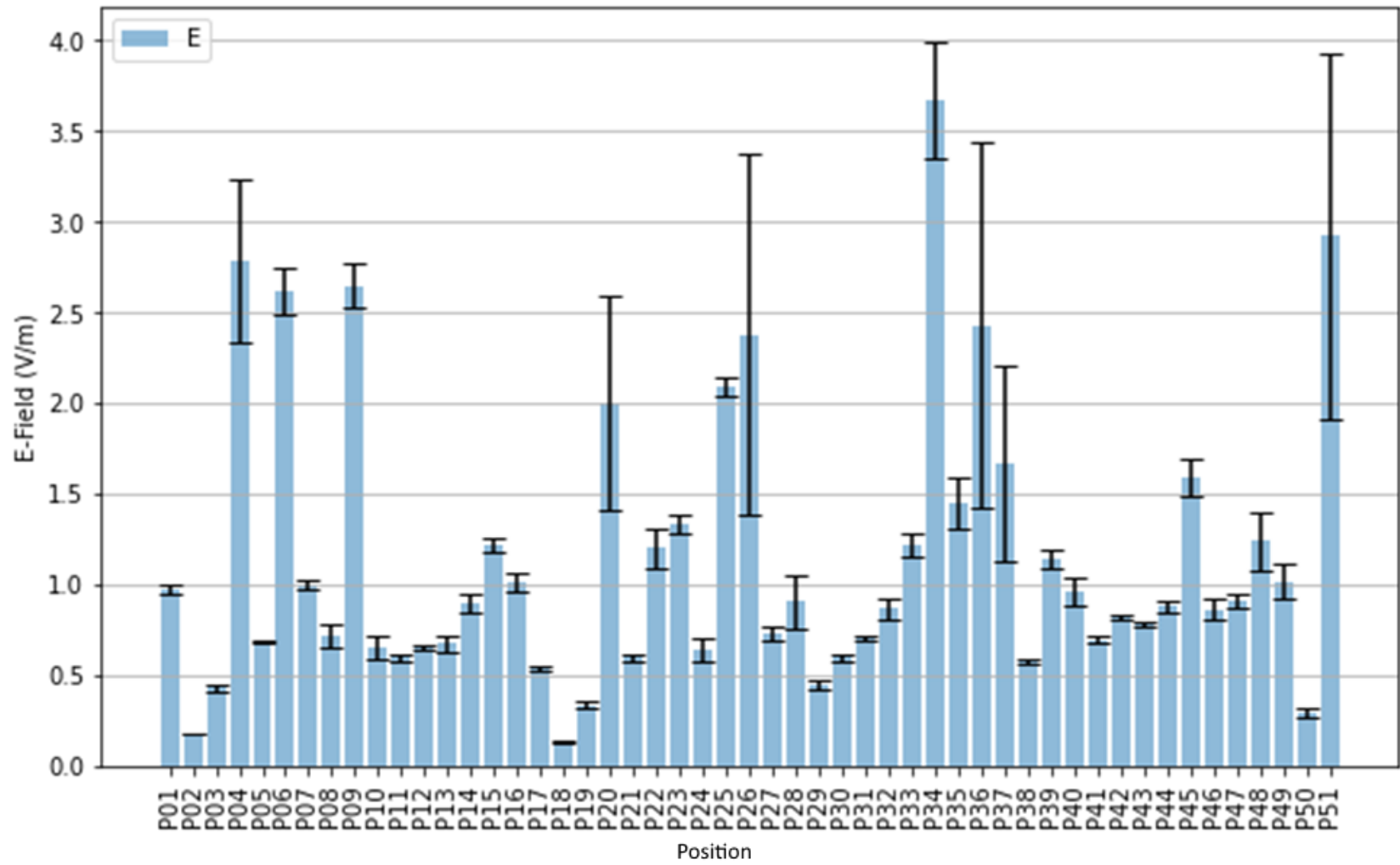


Fig. 5.5. Total exposure levels at various positions in Nairobi CBD.

From the directional variability perspective, the measurements obtained showed that electric field varies based on both direction and distance from BTS. While the highest value of electric field was measured at 90 m distance from the BTS, the intensity of electric field reduces with distance from the BTS (see Table 5.5). Furthermore, it was observed that direction from the BTS also affects the intensity of electric field. This observation can be attributed to directionality of the antennas and propagation of electric fields. The intensity is usually high where the main lobe reaches the ground.

Table 5.5: Variation of electric field at various distances and directions

Distance (m)	30	60	90	100	120	150
Direction 1 E-field (V/m)	0.758	1.3042	1.7528	1.1212	1.0171	0.9613
Direction 2 E-field (V/m)	0.3256	0.3492	0.4293	0.5782	0.5496	0.3492
Direction 3 E-field (V/m)	0.4211	0.4211	1.7451	1.0677	0.4211	0.3492

5.3.1 Comparison of residential and CBD RF-EMF measurements

Statistical and visual techniques were used to evaluate the exposure to RF-EMF variation between CBD and residential regions. Fig. 5.6 shows a boxplot of the two regions that was plotted using the median values. From the Fig., it can be shown that the CBD region had a higher median value of exposure to RF-EMF than residential areas. It was also found that the total exposure values within CBD were more widely spread than in the residential regions. WhitneyWilcoxon statistical test was also carried out to show whether there was a statistically significant difference between CBD and residential areas. Performing a t-test to assess the differences between the two samples requires the data to be normally distributed, which was not the case with the data. A non-parametric test was performed to investigate the difference between the two regions. The test showed that at 0.05 significance level, there was no statistically significant difference between electric field exposure in the two regions ($W = 284$, $p\text{-value} = 0.4329$). Another similar pattern observed in the two regions was the contribution to the total exposure values. In both regions, LTE700 and LTE2600 had the lowest contributions.

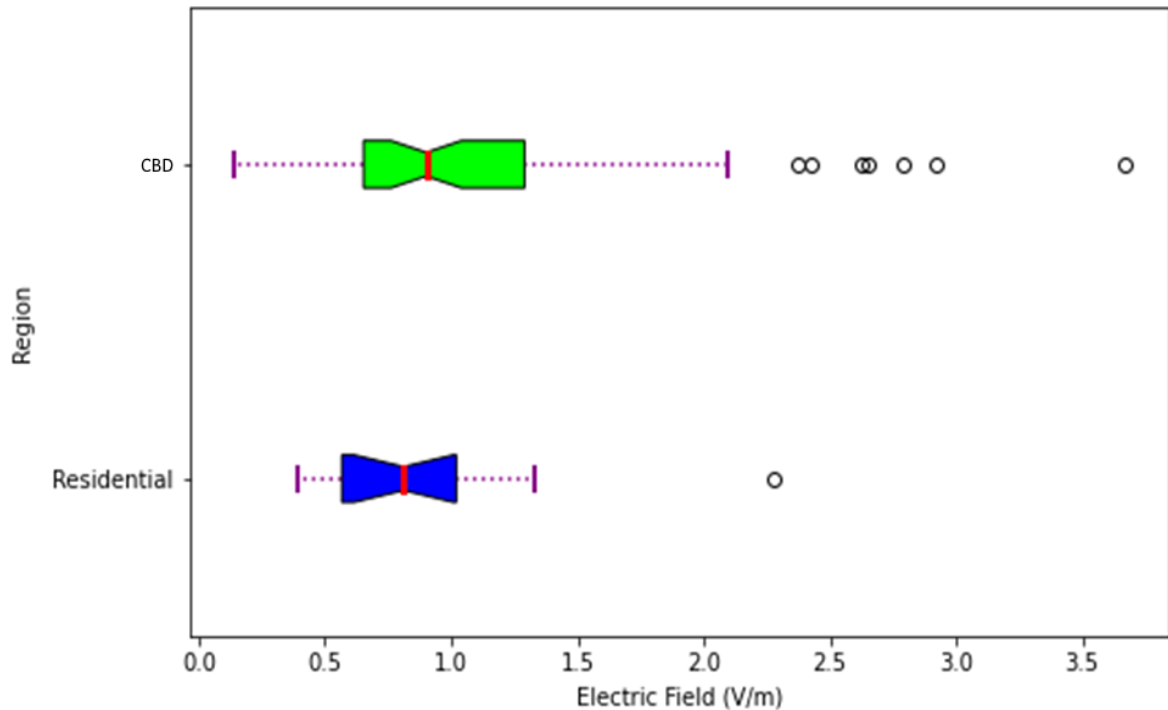


Fig. 5.6: Boxplot of median values of electromagnetic field exposure in CBD and residential areas.

5.3.2 Comparison of the measured RF-EMF values with ICNIRP guidelines

A total exposure quotient (see Equation 3.7) that does not exceed one confirms compliance with the ICNIRP guidelines. The point with the highest total exposure in the two regions was used to establish whether the exposure was within the acceptable limits. Since the radiofrequency signals have additive effects, the total exposure quotient was calculated and found to be 0.000587. Therefore, it was concluded that the exposure to electromagnetic fields is below the limits as provided by the ICNIRP.

5.3.3 Exploratory Analysis of RF-EMF Data

Fig. 5.7 shows the visual representation of the spectra with empty regions after discarding insignificant data. From the Fig., it was confirmed that the data used for the exploratory analysis was associated with relevant frequency bands (see Table 4.1) considered during the study.

Gaps in Frequency Data

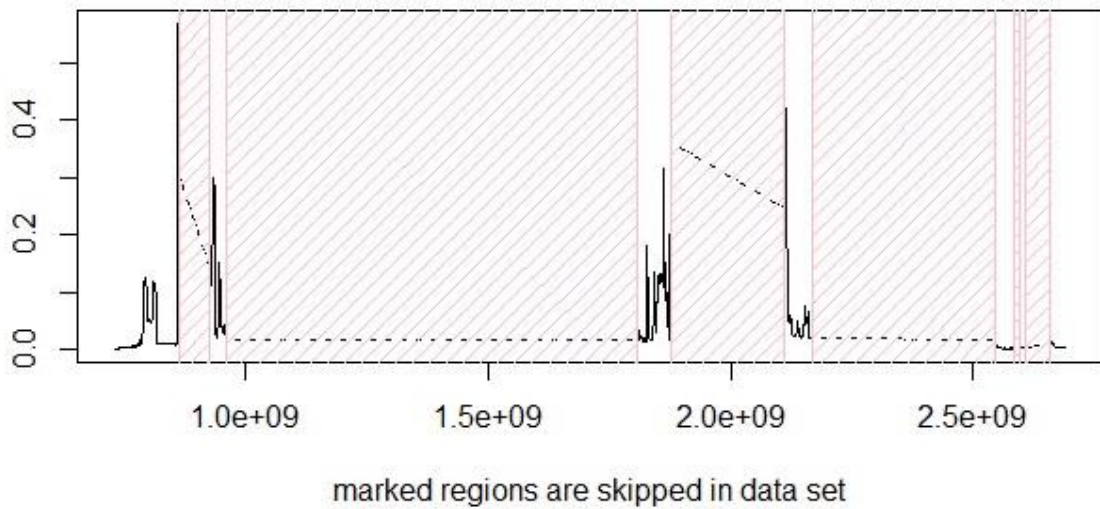


Fig. 5.7: Graphical representations of empty regions.

Fig. 5.8 shows the PCA score plots of the measurements obtained from CBD and residential regions. As there were only 13 residential sites, only 13 out of 51 sites from the CBD were considered (the criteria used in the selection of the sites is described in Section 4.3) in order to balance the number of samples collected from the residential sites. The first and second PC scores were 57 and 18 percent, respectively and cumulatively explaining 74% variation of the data, as shown in Fig. 5.8 (a).

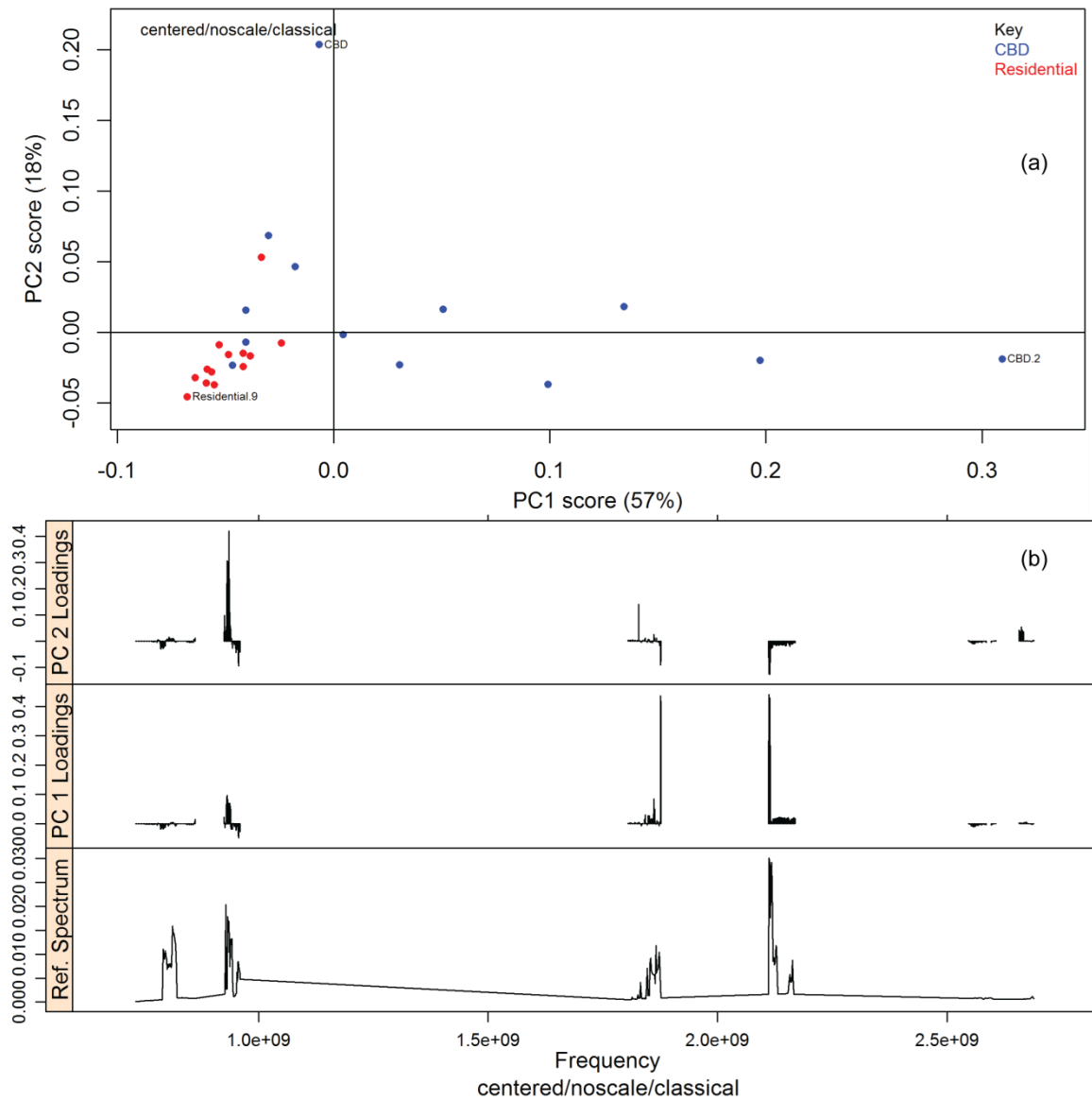


Fig. 5.8: (a) PCA scores plot and (b) PCA loadings plot for the residential and CBD EMF exposure.

Most of the residential measurements are clustered on the lower left quadrant, while most of CBD measurements are grouped on the right-side quadrants for the first two PCs. Fig. 5.8 (b) shows the effects of various frequencies on the scores. Measurements of electric field from the CBD were major contributors of the first principal components as shown by Fig. 5.8 (b). It was also observed that GSM1800 and UMTS2100 were dominant in the CBD region. It was observed that GSM900 had less influence on first principal component than UMTS2100 and GSM1800. On the other hand, GSM 900 was the main contributor of second principal component. The loadings plot showed that GSM900 had a slight negative impact on the second PC and another section of the frequency band had a

great influence on the PC. The other frequency bands were not dominant in both regions. The LTE800 and LTE700 had a slightly negative effect on both PC1 and PC2. The LTE2600 had slight impact on the second PC. From the observations, it can be deduced that GSM900, which is mostly used for mobile calls and sending messages dominated in residential areas whereas UMTS2100 and GSM1800 used for wireless connectivity and, voice call, sending messages dominated in CBD.

Figs. 5.9 (a) and (b) show the s-plots for the first and second PCs showing the individual frequencies with the most influence on the data with the most influential variables.

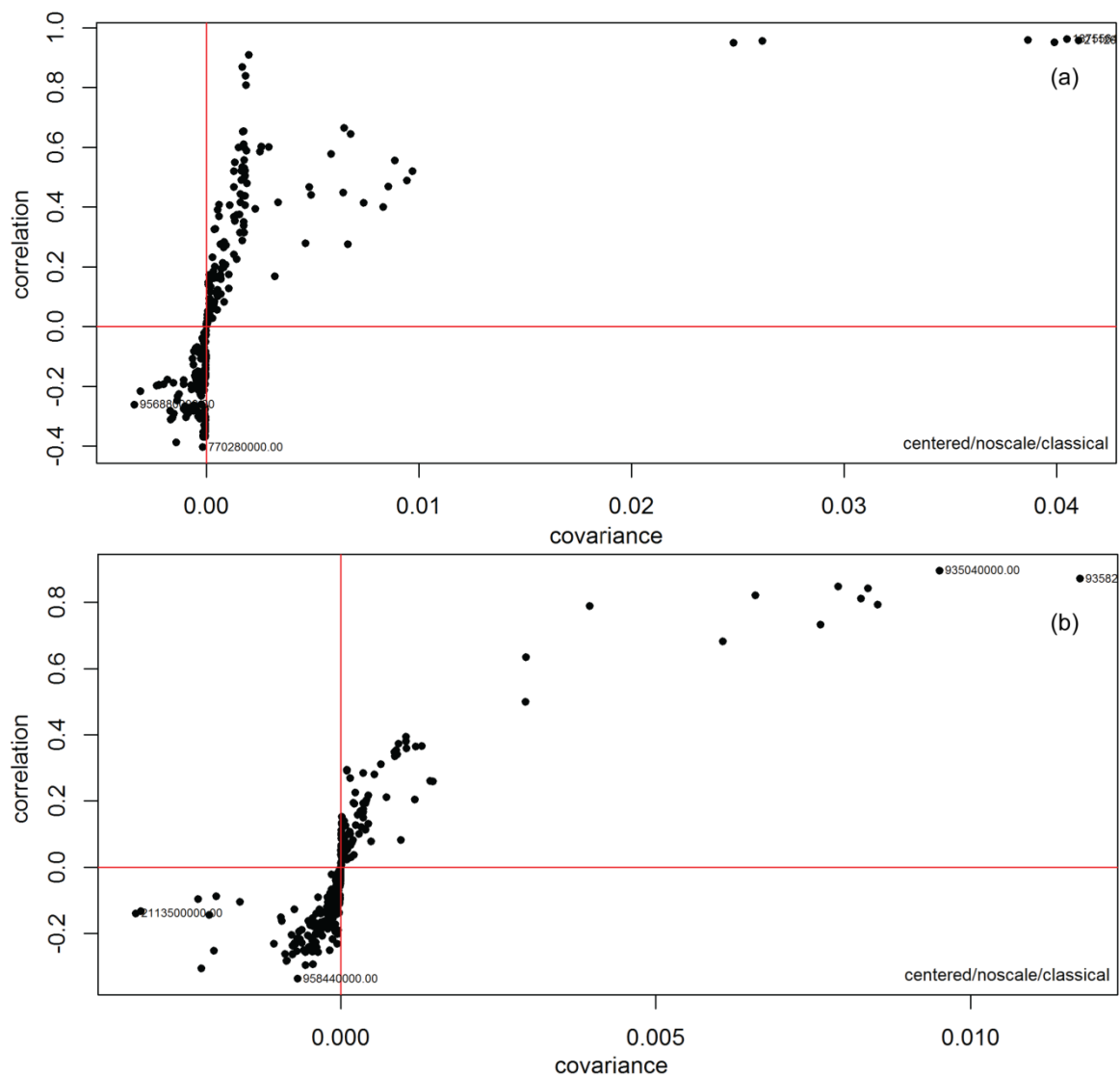


Fig. 5.9: S-plot for (a) PC1 and (b) PC2.

It may be observed that some of the frequencies shown in Fig. 5.8 (a) include 2113, 956, 1877, and 2110 MHz within the GSM900, UMTS2100, and GSM1800 downlink frequency bands. Fig. 5.9 (b) shows frequencies such as 931, 933 MHz, and 935 MHz which are within the GSM900 downlink frequency band. Consequently, it was found that these frequency bands were the most dominant contributors to RF-EMF exposure in the regions where measurements were performed.

5.4 Results of Geospatial Mapping of RF-EMF Levels in the CBD

The variogram (see Fig. 5.10) allowed for visual assessment and spatial correlation modeling. `gstat` package in `r` allowed for fitting the variogram parameters of the spherical model to the sample variogram. The “Sph model” gave the best fit of the variogram with $\text{psill} = 0.6126709$ and $\text{range} = 0.2877821$. The fitted model was used to perform the spatial interpolation. Refer to the appendix 1 for detail of lagged scatter plot.

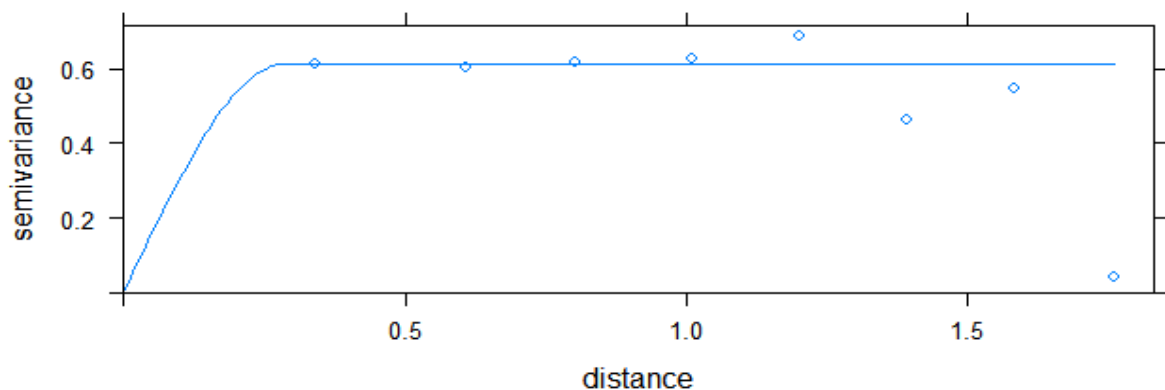


Fig. 5.10: Variogram model used for kriging.

The data mapping was performed to show how the exposure in Nairobi CBD varied from one point to another. The grid over which the kriging was performed is shown in in the Appendix 1. Fig. 5.11 (a) shows the map that resulted after performing ordinary kriging to predict the unknown values of electric field exposure using the measured values. Fig. 5.11 (b) shows the associated interpolated variance values that are normally referred to as kriging prediction errors. A significant part of the region under study exhibits electric field values between 0.5 and 1 V/m. The variance value was approximately $0.7\text{V}^2/\text{m}^2$.

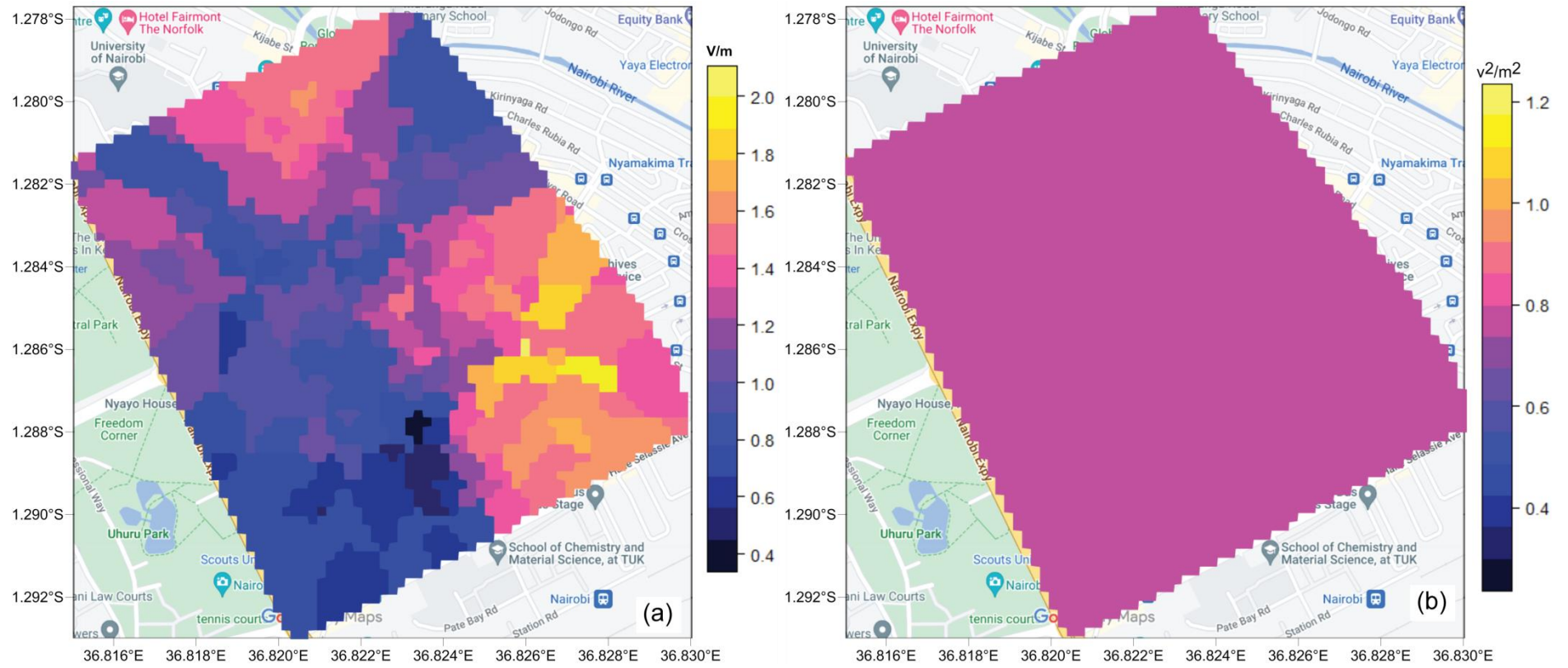


Fig. 5.11: Map of Nairobi CBD indicating (a) interpolated values of RF-EMF exposure and (b) variance of the interpolated EMF measurements.

It was observed that in each of the hotspot areas (i.e. > 1.4 v/m) there was at least one antenna near the measurement point. Some of these sites are shown in Fig. 5.12, and their description is presented on Table 5.5.

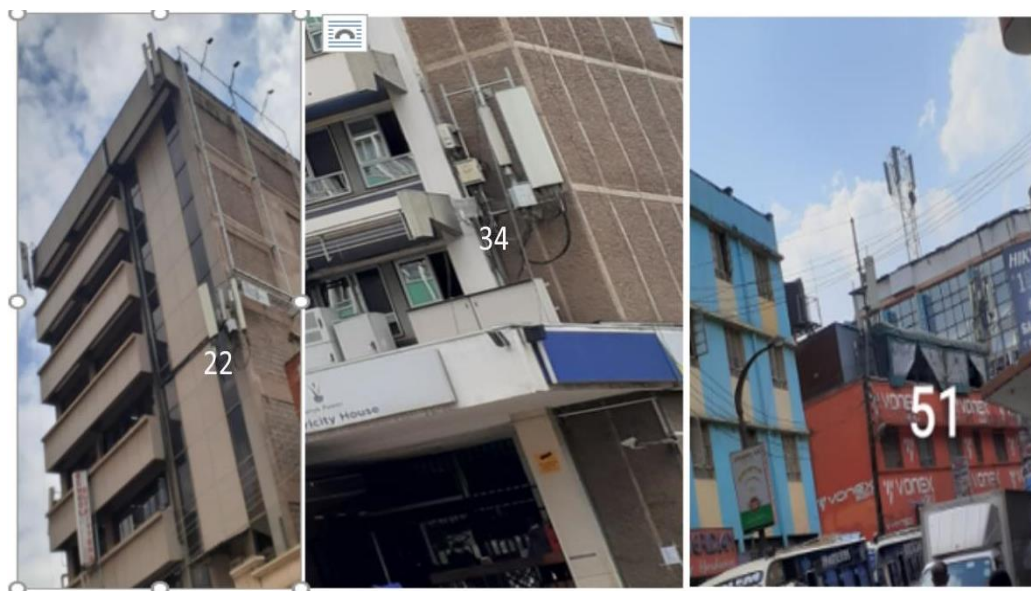


Fig. 5.12: Photos of the three sites that exhibited the highest RF-EMF exposure levels.

Table 5.6: Summary of sites with elevated levels of exposure to EMF fields.

Photo label	Brief Description
22	It is along Muindi Bingu street opposite City Market. The building has several businesses including school outfitters. Several antennas are fixed at various heights on the building.
34	The elevated electric field exposure values resulted from an antenna fixed a few meters from the ground on the Kenya Power building in Nairobi CBD.
51	The data collection point was opposite Pramukh plaza that had an antenna fixed on the wall. Other antennas were shown on the neighboring buildings along Munyu Road.

Fig. 5.13 shows the regions within the CBD that are likely to exceed 2 V/m, generated using the kriging technique. It was found that areas surrounding Bus Station and OTC had

the highest probability compared to areas near the Haile Selassie Avenue and Uhuru High Way roundabout. Furthermore, although some antennas are fixed in hidden places, there were several radiating antenna spotted in the areas with high probability of exceeding 2 V/m. For instance, building neighboring Bus Station had several radiating antennas at the top. Nonetheless, these values are far below the ICNIRP threshold required to cause harm to human tissues.

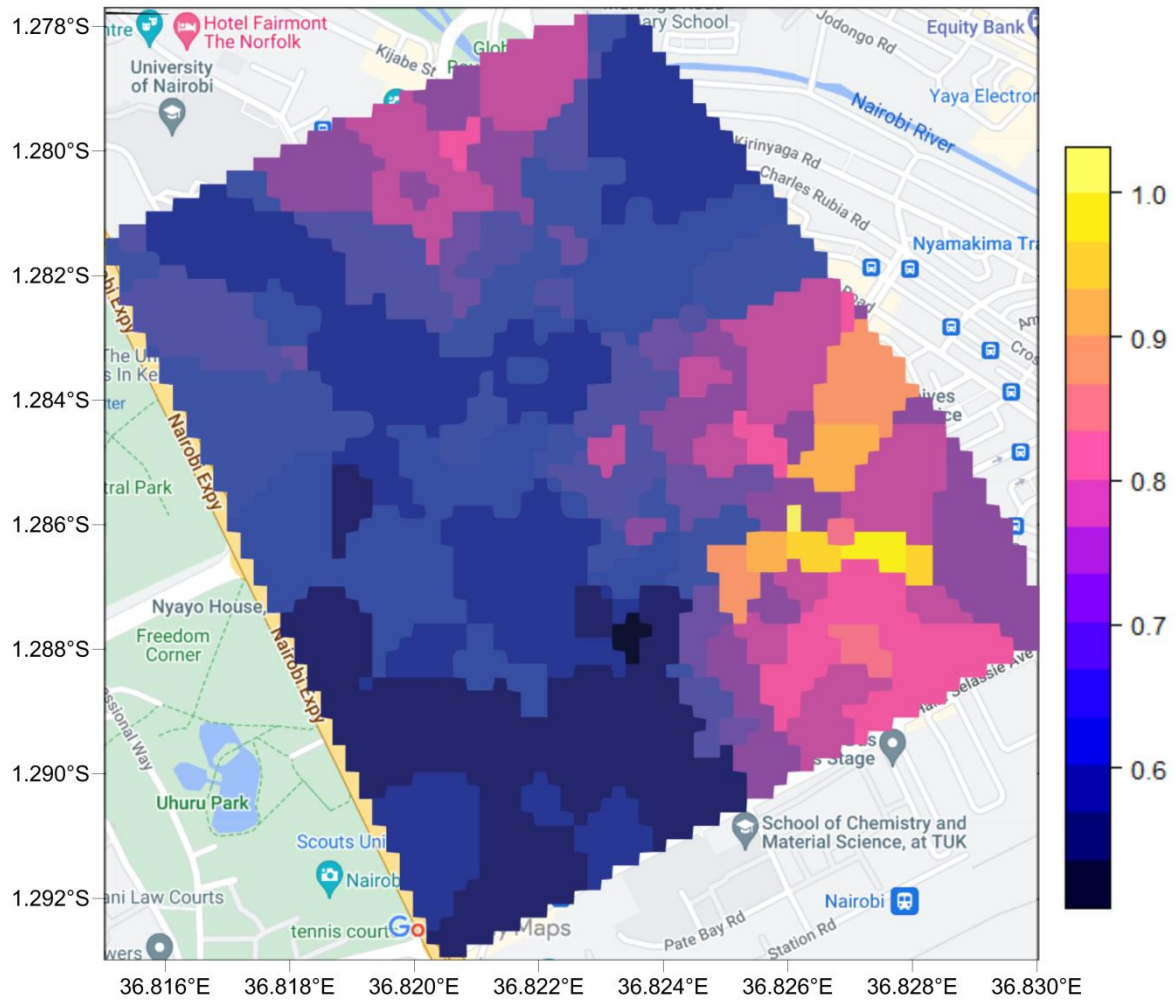


Fig. 5.13: Map of Nairobi CBD indicating the probability of RF-EMF exceeding 2 V/m.

CHAPTER SIX

CONCLUSION AND RECOMMENDATIONS

6.1 Conclusion

There are many studies on non-ionizing radiation exposure conducted in different parts of the world, but such research is limited in Kenya. The assessment of exposure to NIR is essential due to the harmful impacts that are likely to result from overexposure, particularly due to increasing radiofrequency energy applications for domestic and commercial purposes. The use of Spectran Analyzer HF6065 to measure electric field during the study was successful. The different characteristics of electric fields propagation in different settings were also shown. The assessment of NIR using a frequency-selective radiation meter (Spectran Analyzer HF6065) facilitated the identification of the frequency signal with the greatest influence on the exposure to NIR.

The measurement results were further analyzed using appropriate methods to characterize the exposure to electric field associated with telecommunication services. Various library packages in Python were used to analyze the data. The median was found to be the most appropriate parameter to describe the exposure since the data was not normally distributed in most instances. The application of the guidelines provided by the ICNIRP was successful in establishing the status of the exposure levels associated with the application of RF energy. The comparison results showed that the exposure was too low and has not potential hazards to the members of the public. The exploratory analysis of the data enhanced a deeper understanding of the exposure in the considered regions. Various library packages in R-software (*Chemospec*, *sp*, *spplot*, *ggplot2*, *ggmap*) were successful in showing the NIR exposure details in the two regions. Appropriate comparison methods were used to show the differences in exposure to NIR between the two categories (commercial and residential) considered during the study. Comparison between the measured values of electric field with provisions of the ICNIRP showed that the general population within the assessed areas was not overexposed to RF-EMF. The use of total exposure quotient proved to be a successful technique for assessing compliance with ICNIRP limits in a multiple-frequency environment.

The use of the kriging technique to spatialize the data obtained from the study allowed for a 2dimensional visual representation of exposure to EMF fields. Besides, the technique

showed the possibility of using known values to estimate NIR quantities at unmeasured points. Further this approach can be ideal in calculating the probability of exceeding a particular threshold. Spatial interpolation is an important technique in visualization of variables over space. It can also be used to show the variation other quantities in an environment.

Since the exposure levels in Nairobi where there are numerous radiating telecommunication structures are significantly below the NIR exposure limits, it can be deduced that there is a high probability of the exposure being below the limits even in rural areas. However, it would be important for the assessment to be performed in other places in Kenya and assess the status to confidently conclude the status based on verifiable facts. Since NIR exposure is not dependent on telecommunication structures exclusively, it would be important to have more studies to assess the other sources of NIR in the country to ensure that members of the public are not overexposed to any type of NIR. Also, data mapping using geostatistical techniques can be used in different residential areas to present 2-dimensional maps of the exposure to electromagnetic fields. Regular assessment of NIR in all parts of the country is necessary to ensure that the people are not overexposed to NIR despite the ever-increasing applications of RF energy.

6.2 Recommendations

There is need for more work to be done in Kenya to ensure that the exposure associated with NIR does not exceed the limits as provided by the ICNIRP. Although the electric field values associated with telecommunication structures surveyed in this study were within the acceptable limits, more research is necessary to inform the status of exposure associated with other sources of NIR. For instance, the high-voltage power cables, radar systems, etc. should be assessed to ascertain their contribution to NIR exposure to the general public. It is also important to consider occupational worker in future studies.

Furthermore, the population in other developing towns and cities is increasing continuously and telecommunication services providers proportionately install more BTS to meet the network demands. Therefore, it is important to perform regular survey particularly in these areas to ensure that the members of the public are not overexposed to electromagnetic fields and NIR.

REFERENCES

- Aaronia (2013), *HW V4 © 2005-2013 Wwww.Aaronia.Com 2 Manual Spectran V4*, available at:https://doi.org/https://www.aaronia.com/Datasheets/Documents/SPECTRAN-HF_V4_EN.pdf.
- Abzalov, M. (2016), Introduction to geostatistics, *Mod. Approaches Solid Earth Sci.*, Vol. 12, pp. 233–237.
- Aerts, S., Deschrijver, D., Verloock, L., Dhaene, T., Martens, L. and Joseph, W. (2013), Assessment of outdoor radiofrequency electromagnetic field exposure through hotspot localization using kriging-based sequential sampling, *Environ. Res.*, Academic Press Inc., **Vol. 126**, pp. 184–191.
- Aerts, S., Wiart, J., Martens, L. and Joseph, W. (2018), Assessment of long-term spatio-temporal radiofrequency electromagnetic field exposure, *Environ. Res.*, **Vol. 161**, available at:<https://doi.org/10.1016/j.envres.2017.11.003>.
- Ajiboye, Y. and Osiele, M.O. (2013), Assessment of Spatial Exposure to RF Radiation due to GSM 900 and GSM1800 – A Case Study of UCH, Ibadan, Nigeria, *IOSR J. Appl. Phys.*, **Vol. 4 No. 2**.
- Alasadi, S.A. and Bhaya, W.S. (2017), Review of data preprocessing techniques in data mining, *J. Eng. Appl. Sci.*, **Vol. 12 No. 16**, available at:<https://doi.org/10.3923/jeasci.2017.4102.4107>.
- Ali, M., Goovaerts, P., Nazia, N., Haq, M.Z., Yunus, M. and Emch, M. (2006), Application of Poisson kriging to the mapping of cholera and dysentery incidence in an endemic area of Bangladesh, *Int. J. Health Geogr.*, **Vol. 5**, available at:<https://doi.org/10.1186/1476-072X-5-45>.
- Azpurua, M. and dos Ramos, K. (2010), A comparison of spatial interpolation methods for estimation of average electromagnetic field magnitude, *Prog. Electromagn. Res. M*, available at:<https://doi.org/10.2528/PIERM10083103>.
- Bekele, A., Downer, R.G., Wolcott, M.C., Hudnall, W.H. and Moore, S.H. (2003), Comparative evaluation of spatial prediction methods in a field experiment for mapping soil potassium, *Soil Sci.*, **Vol. 168 No. 1**, available at:<https://doi.org/10.1097/00010694-200301000-00003>.
- Breckenkamp, J., Neitzke, H.P., Bornkessel, C. and Berg-Beckhoff, G. (2008),

- Applicability of an exposure model for the determination of emissions from mobile phone base stations, *Radiat. Prot. Dosimetry*, **Vol. 131 No. 4**, available at:<https://doi.org/10.1093/rpd/ncn201>.
- Buckus, R., Strukčinskienė, B., Raistenskis, J., Stukas, R., Šidlauskienė, A., Čerkauskienė, R., Isopescu, D.N., *et al.* (2017), A technical approach to the evaluation of radiofrequency radiation emissions from mobile telephony base stations, *Int. J. Environ. Res. Public Health*, available at:<https://doi.org/10.3390/ijerph14030244>.
- Câmara, P. (2014), Effect of Exposure to Non-ionizing Radiation (Electromagnetic Fields) on Human System: A Literature Review, *J. Interdiscip. Histopathol.*, ScopeMed International Medical Journal Management and Indexing System, **Vol. 2 No. 4**, p. 187.
- Chiaromello, E., Bonato, M., Fiocchi, S., Tognola, G., Parazzini, M., Ravazzani, P. and Wiart, J. (2019), Radio frequency electromagnetic fields exposure assessment in indoor environments: A review, *Int. J. Environ. Res. Public Health*, available at:<https://doi.org/10.3390/ijerph16060955>.
- Communication Authority Of Kenya. (2020), Second Quarter Sector Statistics Report for the Financial Year, *Second Quart. Sect. Stat. Rep. Financ. Year*, **Vol. 2020 No. December 2019**, pp. 1–24.
- Communications Authority of Kenya. (2018), *Features and Technical Specifications for Mobile Cellular Devices - Kenya*, available at: <https://www.ca.go.ke/wp-content/uploads/2018/06/Guidelines-on-the-Minimum-Features-and-Technical-Specifications-for-Mobile-Cellular-Devices-Imported-into-and-Distributed-in-Kenya-June-2018.pdf>.
- Enyinna, P.I. and Avwir, G.O. (2010), Characterization of the radiofrequency radiation potential of Alakahia and Choba communities, Nigeria, **Vol. 7 No. 1**, pp. 25–31.
- Gajsek, P., Struchen, B. and Valid, B. (2016), RF exposure survey of children and adults: First results from Slovenia, *2016 IEEE Radio Antenna Days Indian Ocean. RADIO 2016*, available at:<https://doi.org/10.1109/RADIO.2016.7772027>.
- Hanson, B.A. (2018), An Introduction to ChemoSpec, *ChemoSpec*.
- ICNIRP. (2020), Guidelines for limiting exposure to electromagnetic fields (100 kHz to 300 GHz). International Commission on Non-Ionizing Radiation Protection, *Health Phys.*, **Vol. 118 No. 5**.

- Ikechukwu, M.N., Ebinne, E., Idorenyin, U. and Raphael, N.I. (2017), Accuracy Assessment and Comparative Analysis of IDW, Spline and Kriging in Spatial Interpolation of Landform (Topography): An Experimental Study, *J. Geogr. Inf. Syst.*, **Vol. 09 No. 03**, available at:<https://doi.org/10.4236/jgis.2017.93022>.
- ITU. (2015), *ITU-T Generation of Radio-Frequency Electromagnetic Field Level Maps Recommendation ITU-T K.113*, available at: <http://handle.itu.int/11.1002/1000/11>.
- Joseph, W., Frei, P., Roösli, M., Thuróczy, G., Gajsek, P., Trcek, T., Bolte, J., *et al.* (2010), Comparison of personal radio frequency electromagnetic field exposure in different urban areas across Europe, *Environ. Res.*, available at:<https://doi.org/10.1016/j.envres.2010.06.009>.
- Kang, H. (2013), The prevention and handling of the missing data, *Korean J. Anesthesiol.*, available at:<https://doi.org/10.4097/kjae.2013.64.5.402>.
- Bin Khuzairi, K., Rahim, H.A., Abdulmalek, M. and Warip, M.N.B.M. (2019), Radio frequency radiation measurement for base tower station safety compliances: A case study in Pulau Pinang Malaysia, *Bull. Electr. Eng. Informatics*, **Vol. 8 No. 1**, available at:<https://doi.org/10.11591/eei.v8i1.1407>.
- KNBS. (2019), *Kenya Population and Housing Census Volume 1: Population by County and Sub-County*, *Kenya Natl. Bur. Stat.*, Vol. I, available at: <https://www.knbs.or.ke/?wpdmpro=2019-kenya-population-and-housing-census-volume-i-population-by-county-and-sub-county>.
- Kravchenko, A.N. (2003), Influence of Spatial Structure on Accuracy of Interpolation Methods, *Soil Sci. Soc. Am. J.*, **Vol. 67 No. 5**, available at:<https://doi.org/10.2136/sssaj2003.1564>.
- Kurnaz, Ç. and Korunur Engiz, B. (2016), Measurement and Evaluation of Electric Field Strength in Samsun City Center, *Int. J. Appl. Math. Electron. Comput.*, International Journal of Applied Mathematics, Electronics and Computers, **Vol. 4 No. Special Issue-1**, pp. 24–24.
- Lahham, A. and Hammash, A. (2012), Outdoor radiofrequency radiation levels in the West Bank-palestine, *Radiat. Prot. Dosimetry*, **Vol. 149 No. 4**, pp. 399–402.
- Lark, R.M., Cullis, B.R. and Welham, S.J. (2006), On spatial prediction of soil properties in the presence of a spatial trend: The empirical best linear unbiased predictor (E-BLUP) with REML, *Eur. J. Soil Sci.*, **Vol. 57 No. 6**, available

at:<https://doi.org/10.1111/j.1365-2389.2005.00768.x>.

- Lopa, M. and Vora, J. (2015), Evolution of mobile generation technology: 1G to 5G, *Int. J. Mod. Trends Eng. Res.*, **Vol. 02**, pp. 281–291.
- Mann, S.M.. C.T.G.. A.S.G.. B.R.P.& L.A.. J.G.B.N.R.P.B. (2000), *Exposure to Radio Waves near Mobile Phone Base Stations*, National Radiological Protection Board.
- Matheron, G. (1971), Matheron, G. (1971) The Theory of Regionalized Variables and Its Applications. Les Cahiers du Centre de Morphologie Mathematique in Fontainebleu, Paris., *Sci. Res.*
- Maxwell, J.C. (1998), Fundamentals of electromagnetism, *Mod. Antennas*, pp. 1–24.
- Meng, Q., Liu, Z. and Borders, B.E. (2013), Assessment of regression kriging for spatial interpolation - Comparisons of seven GIS interpolation methods, *Cartogr. Geogr. Inf. Sci.*, **Vol. 40 No. 1**, available at:<https://doi.org/10.1080/15230406.2013.762138>.
- Mohebzadeh, H. (2018), Comparison of Methods for Fitting the Theoretical Variogram to the Experimental Variogram for Estimation of Depth to Groundwater and its Temporal and Spatial Variations, available at:<https://doi.org/10.5829/idosi.aejaes.2018.64.76>.
- Mueller, T.G., Pierce, F.J., Schabenberger, O. and Warncke, D.D. (2001), Map Quality for Site-Specific Fertility Management, *Soil Sci. Soc. Am. J.*, **Vol. 65 No. 5**, available at:<https://doi.org/10.2136/sssaj2001.6551547x>.
- Ozen, S., Helhel, S. and Colak, O.H. (2007), Electromagnetic field measurements of radio transmitters in urban area and exposure analysis, *Microw. Opt. Technol. Lett.*, **Vol. 49 No. 7**, available at:<https://doi.org/10.1002/mop.22548>.
- Paniagua, J.M., Rufo, M., Jimenez, A. and Antolin, A. (2013), The spatial statistics formalism applied to mapping electromagnetic radiation in urban areas, *Environ. Monit. Assess.*, **Vol. 185 No. 1**, available at:<https://doi.org/10.1007/s10661-012-2555-7>.
- R Core Team. (2021), R Core Team 2021 R: A language and environment for statistical computing. R foundation for statistical computing. <https://www.R-project.org/>, *R Found. Stat. Comput.*
- Rowley, J.T. and Joyner, K.H. (2012), Comparative international analysis of radiofrequency exposure surveys of mobile communication radio base stations, *J. Expo. Sci. Environ. Epidemiol.*, **Vol. 22 No. 3**, available

- at:<https://doi.org/10.1038/jes.2012.13>.
- Sagar, S., Adem, S.M., Struchen, B., Loughran, S.P., Brunjes, M.E., Arangua, L., Dalvie, M.A., *et al.* (2018), Comparison of radiofrequency electromagnetic field exposure levels in different everyday microenvironments in an international context, *Environ. Int.*, **Vol. 114**, available at:<https://doi.org/10.1016/j.envint.2018.02.036>.
- Santini, R., Santini, P., Danze, J.M., Le Ruz, P. and Seigne, M. (2002), [Investigation on the health of people living near mobile telephone relay stations: I/Incidence according to distance and sex]., *Pathol. Biol. (Paris)*., **Vol. 50 No. 6**.
- Saravanamuttu, S., Singh, V., Khumukcham, R. and Dorairaj, S. (2015), *A Case Study of Cellular Base Stations in an Indian Metro (Chennai)*, available at: <http://www.sedindia.org>.
- Schloeder, C.A., Zimmerman, N.E. and Jacobs, M.J. (2001), Comparison of Methods for Interpolating Soil Properties Using Limited Data, *Soil Sci. Soc. Am. J.*, **Vol. 65 No. 2**, available at:<https://doi.org/10.2136/sssaj2001.652470x>.
- Staebler, P. (2017), *Human Exposure to Electromagnetic Fields: From Extremely Low Frequency (ELF) To Radiofrequency*, *Hum. Expo. to Electromagn. Fields From Extrem. Low Freq. to Radiofreq.*, available at:<https://doi.org/10.1002/9781119384533>.
- Varmuza, K. and Filzmoser, P. (2009), Multivariate Data, *Introd. to Multivar. Stat. Anal. Chemom.*, available at:<https://doi.org/10.1201/9781420059496.ch2>.
- Vermeeren, G., Markakis, I., Goeminne, F., Samaras, T., Martens, L. and Joseph, W. (2013), Spatial and temporal RF electromagnetic field exposure of children and adults in indoor micro environments in Belgium and Greece, *Prog. Biophys. Mol. Biol.*, available at:<https://doi.org/10.1016/j.pbiomolbio.2013.07.002>.
- Wu, Y.-H. (Eva) and Hung, M.-C. (2016), Comparison of Spatial Interpolation Techniques Using Visualization and Quantitative Assessment, *Appl. Spat. Stat.*, available at:<https://doi.org/10.5772/65996>.
- Yakymenko, I., Sidorik, E., Kyrylenko, S. and Chekhun, V. (2011), Long-term exposure to microwave radiation provokes cancer growth: Evidences from radars and mobile communication systems, *Exp. Oncol.*
- Yao, X., Fu, B., Lü, Y., Sun, F., Wang, S. and Liu, M. (2013), Comparison of Four Spatial Interpolation Methods for Estimating Soil Moisture in a Complex Terrain Catchment,

PLoS One, **Vol. 8 No. 1**, available at:<https://doi.org/10.1371/journal.pone.0054660>.
Zelege, B.M., Brzozek, C., Bhatt, C.R., Abramson, M.J., Croft, R.J., Freudenstein, F.,
Wiedemann, P., *et al.* (2018), Personal exposure to radio frequency electromagnetic
fields among Australian adults, *Int. J. Environ. Res. Public Health*, available
at:<https://doi.org/10.3390/ijerph15102234>.

APPENDICES

Appendix 1: R Code for Kriging

```
library(dplyr)
```

```
##
```

```
## Attaching package: 'dplyr'
```

```
## The following objects are masked from 'package:stats':
```

```
##
```

```
## filter, lag
```

```
## The following objects are masked from 'package:base':
```

```
##
```

```
## intersect, setdiff, setequal, union
```

```
library(gstat)
```

```
library(ggmap)
```

```
## Loading required package: ggplot2
```

```
## Google's Terms of Service: https://cloud.google.com/maps-platform/terms/.
```

```
## Please cite ggmap if you use it! See citation("ggmap") for details.
```

```
library(mapview)
```

```
library(sf)
```

```
## Linking to GEOS 3.9.0, GDAL 3.2.1, PROJ 7.2.1
```

```
library(sp)
```

```
library(viridis)
```

```
## Loading required package: viridisLite
```

```
cbds<-read.csv("C:\\Users\\User\\Desktop\\RADIOFREQUENCY\\DTAS\\The Total  
Exposure Values.csv") cbds <- dplyr::select(cbds, c(2,3,4)) colnames(cbds) <- c("lat",  
"lon", "Exposure") head(cbds)
```

```
## lat lon Exposure
```

```
## 1 -1.292990 36.82051 0.9717254
```



```
## 2 -1.291423 36.81976 0.1810118
```

```
## 3 -1.289814 36.81898 0.4338193
```

```
## 4 -1.288194 36.81815 2.7870731
```

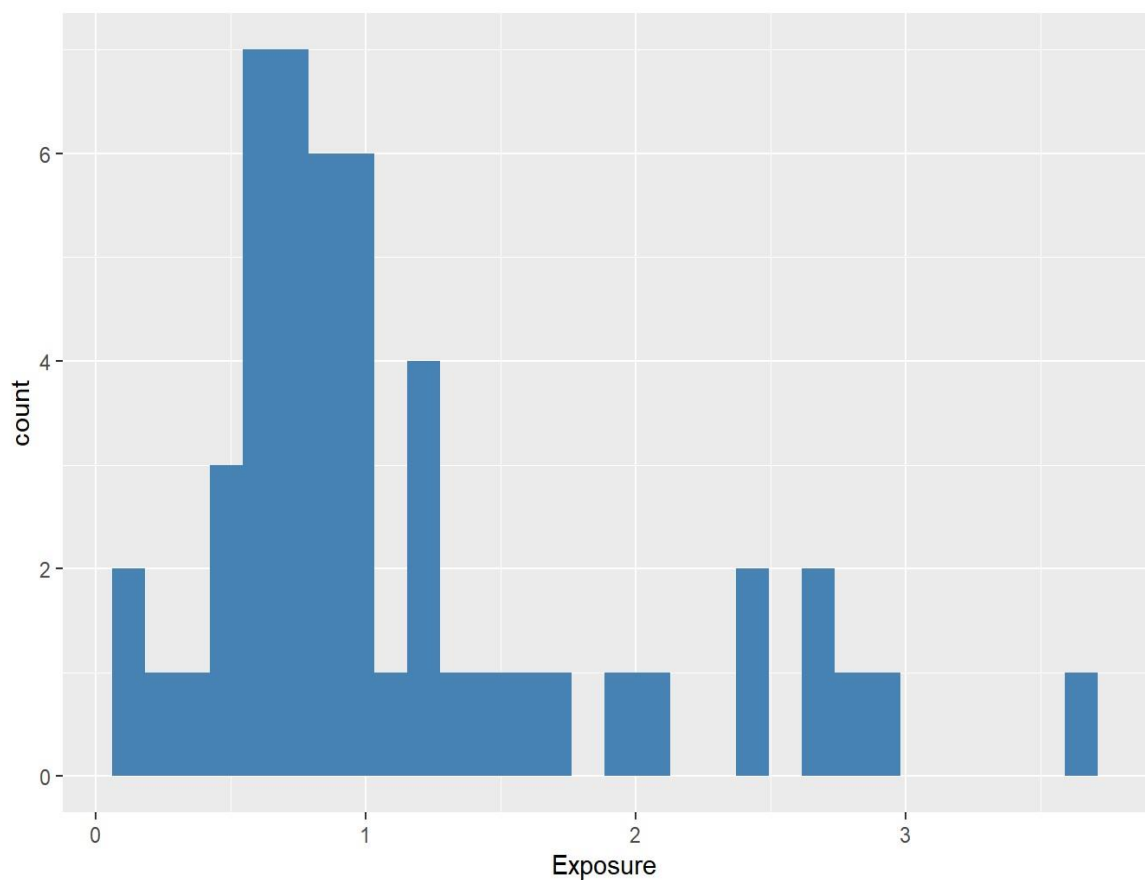
```
## 5 -1.286585 36.81739 0.6886724
```

```
## 6 -1.284934 36.81658 2.6225318
```

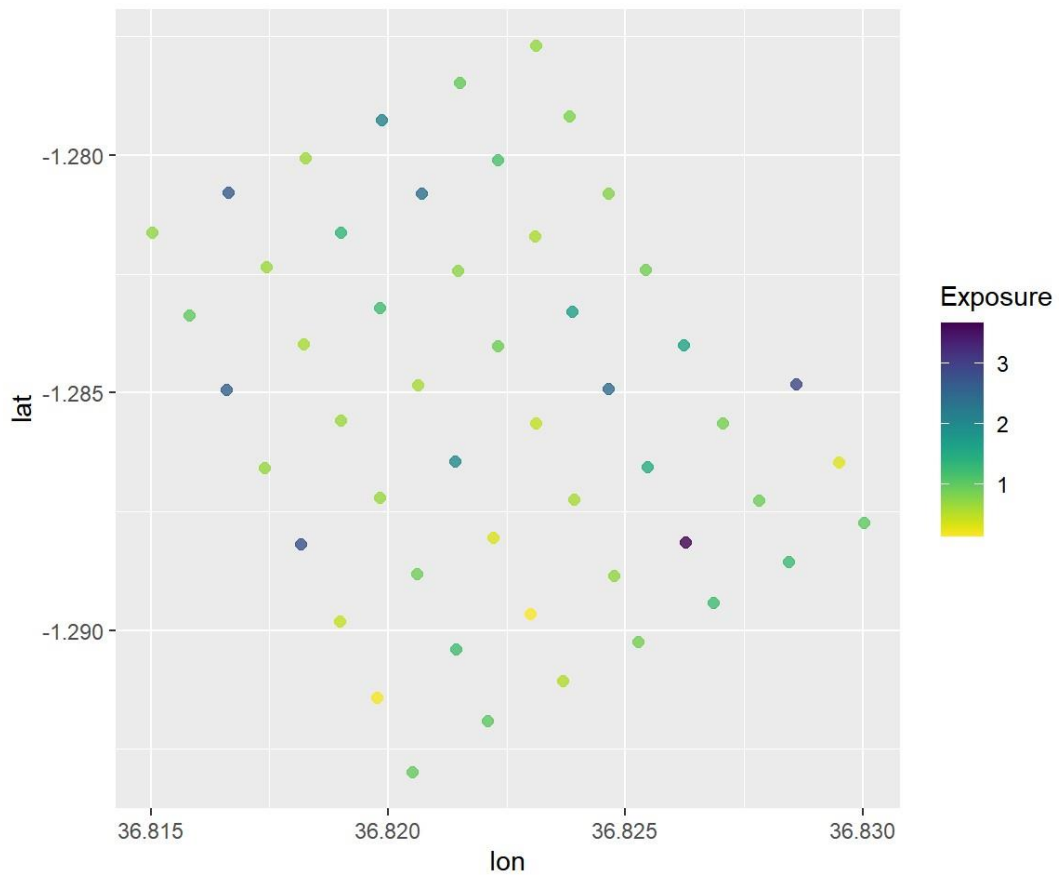
```
ggplot(cbd, mapping = aes(x = Exposure)) +
```

```
  geom_histogram(fill = "steelblue")
```

```
## `stat_bin()` using `bins = 30`. Pick better value with `binwidth`.
```



```
ggplot(cbd, mapping = aes(x = lon, y = lat)) +  
  geom_point(aes(color = Exposure), alpha = .8, size = 2) +  
  scale_color_viridis(direction = -1) + coord_quickmap()
```



```

# Convert our data/subset to a "sf" package "compatible" object
# with associated crs (Coordinate Reference System - further details later on )
# and specifying "lon" and "lat" columns in original dataset
# subset <- st_as_sf(subset, coords = c("lon", "lat"), crs = 4326)
# Create an interactive map with "mapview" function from the "mapview" package
# - zcol: variable to be colour encoded
# - map.types: base layer (here Esri satellite imagery)
# - legend: do we want a legend or not
cbds_sf <- st_as_sf(cbds,
coords = c("lon", "lat"), crs = 4326)
mapview(cbds_sf, zcol = "Exposure", map.types = "Esri.WorldImagery", legend =
TRUE)

```



s_sf - Exposure

.01.52.02.53.03.5

300m
1000ft

cbds_sf- Exposure

[Leaflet](#) | Tiles © Esri, Source: Esri, DeLorme, USDA, USGS, AEX, GeoEye, Getmapping, Aerogrid, IGN, IGP, Swisstopo, and the GIS User Community

```
register_google(key = "AIzaSyCoatSJG9N2kNxoMLU1DekD37z1B9ap0")

cbdsmap <- get_map(location = c(6.8222652745098, -1.28530203921569), maptype = "satellite", zoom = 15)

## Source :https://maps.googleapis.com/maps/api/staticmap?center=285302,36.822265&zoom=15&size=640x640&scale=2&maptype=satellite&language=en&key=xx-cNxoMLU1DekD37z1B9ap0

# Overlay data based on lat and lon attributes

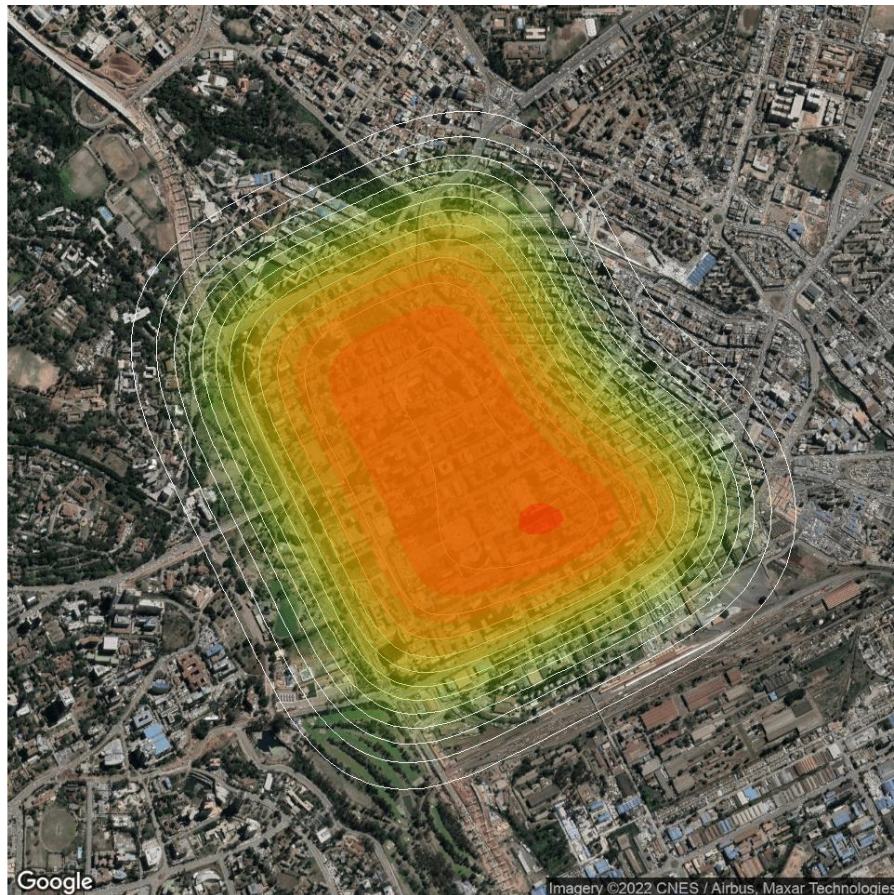
ggmap(cbdsmap, extent = "device") +

  geom_point(aes(x = lon, y = lat), colour = "red", alpha = 0.8, size = 2.5, data = cbds)
```



```
ggmap(cbdsmap, extent = "device") +
```

```
geom_density2d(data = cbds, aes(x = lon, y = lat), size = 0.3, colour = "white") +
stat_density2d(data = cbds, aes(x = lon, y = lat, fill = ..level.., alpha =
..level..),
size = 0.01, bins = 16, geom = "polygon") + scale_fill_gradient(low =
"green", high = "red") + scale_alpha(range = c(0, 0.3), guide = "none")+
guides(fill="none")
```



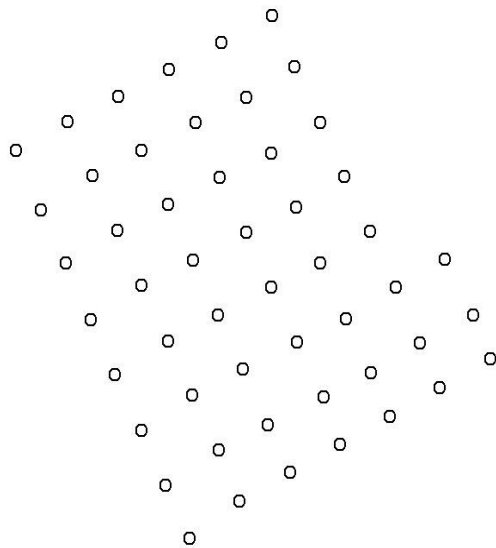
```
cbds_sf <- st_as_sf(cbds, coords = c("lon", "lat"), crs = 4326) cbds_sf

## Simple feature collection with 51 features and 1 field
## Geometry type: POINT
## Dimension: XY
## Bounding box: xmin: 36.81502 ymin: -1.29299 xmax: 36.83004 ymax: -1.27769
## Geodetic CRS: WGS 84
```

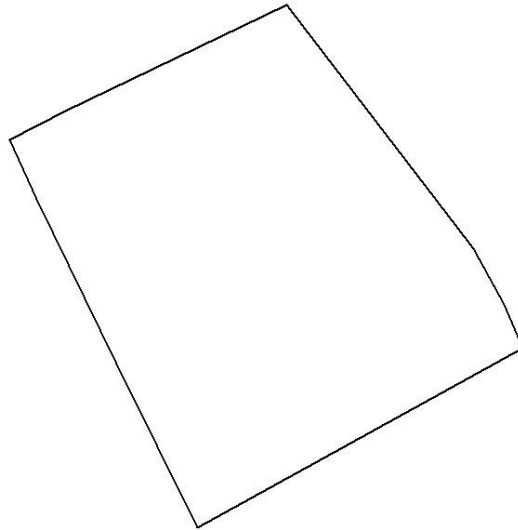
```
## First 10 features:
```

```
## Exposure geometry
## 1 0.9717254 POINT (36.82051 -1.29299)
## 2 0.1810118 POINT (36.81976 -1.291423)
## 3 0.4338193 POINT (36.81898 -1.289814)
## 4 2.7870731 POINT (36.81815 -1.288194)
## 5 0.6886724 POINT (36.81739 -1.286585)
## 6 2.6225318 POINT (36.81658 -1.284934)
## 7 1.0003017 POINT (36.8158 -1.283358)
## 8 0.7169356 POINT (36.81502 -1.281631)
## 9 2.6485655 POINT (36.81664 -1.280789)
## 10 0.6538416 POINT (36.81743 -1.282355)
```

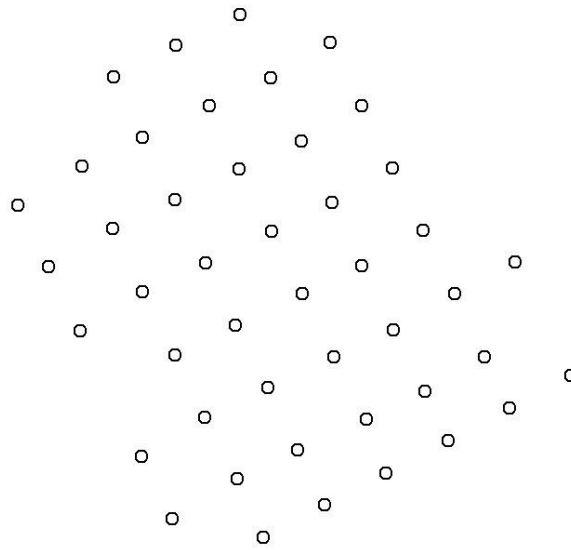
```
plot(st_geometry(cbds_sf))
```



```
cbds_perimeter <- st_convex_hull(st_union(cbds_sf))  
plot(cbds_perimeter)
```



```
st_area(cbds_perimeter)  
## 1563164 [m^2]  
cbdata<-st_as_sf(cbds, coords = c("lon", "lat"), crs = 4326) cbdonly <-  
st_intersection(cbdata, cbds_perimeter)  
## Warning: attribute variables are assumed to be spatially constant througho  
ut all  
## geometries  
plot(st_geometry(cbdonly))
```



```

cbds_utm <- st_transform(cbdsonly, crs = 32633) bboxcbd_utm
<- st_bbox(cbds_utm)
print("Delta X max
(m)")
## [1] "Delta X max (m)"
print(unnamed(bboxcbd_utm[3] - bboxcbd_utm[1]))
## [1] 1701.938
print("Delta Y max (m)")
## [1] "Delta Y max (m)"
print(unnamed(bboxcbd_utm[4] - bboxcbd_utm[2]))
## [1] 1601.565
maximum_pts <- cbds_utm[cbds_utm$Exposure ==
max(cbds_utm$Exposure),]$geometry
cbds_utm <- cbds_utm %>%
mutate(distance = st_distance(geometry, maximum_pts))

```

```
cbds_sp <- as(cbds_utm, Class = "Spatial") head(cbds_sp)
```

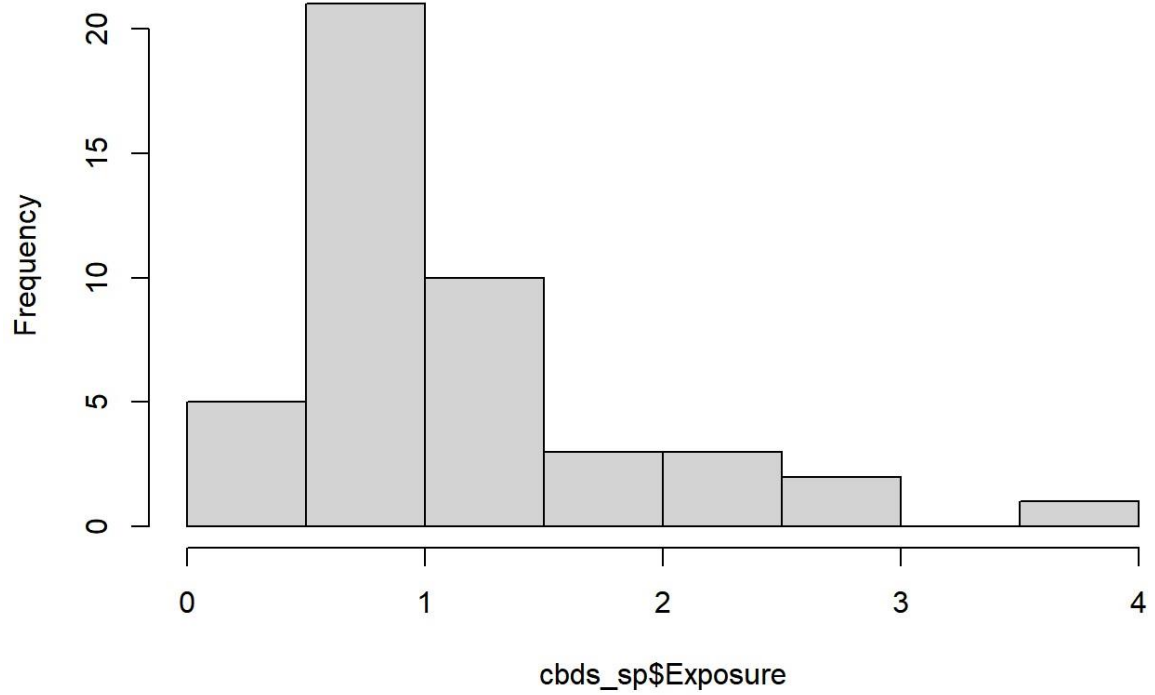
```
## class      : SpatialPointsDataFrame
## features   : 6
## extent     : 2988182, 2988648, -153835.7, -152753.1 (xmin, xmax, ymin, ymax)
## crs        : +proj=utm +zone=33 +datum=WGS84 +units=m +no_defs
## variables  : 2
## names      : Exposure, distance
## min values : 0.18101182, 871.830520799686
## max values : 2.622531822, 1377.3810934017
```

```
tail(cbds_sp)
```

```
## class      : SpatialPointsDataFrame
## features   : 6
## extent     : 2989430, 2989884, -153504.8, -152957.9 (xmin, xmax, ymin, ymax)
## crs        : +proj=utm +zone=33 +datum=WGS84 +units=m +no_defs
## variables  : 2
## names      : Exposure, distance
## min values : 0.863147019, 213.031804699424
## max values : 2.922255194, 494.034727861268
```

```
hist(cbds_sp$Exposure)
```


Histogram of cbds_sp\$Exposure

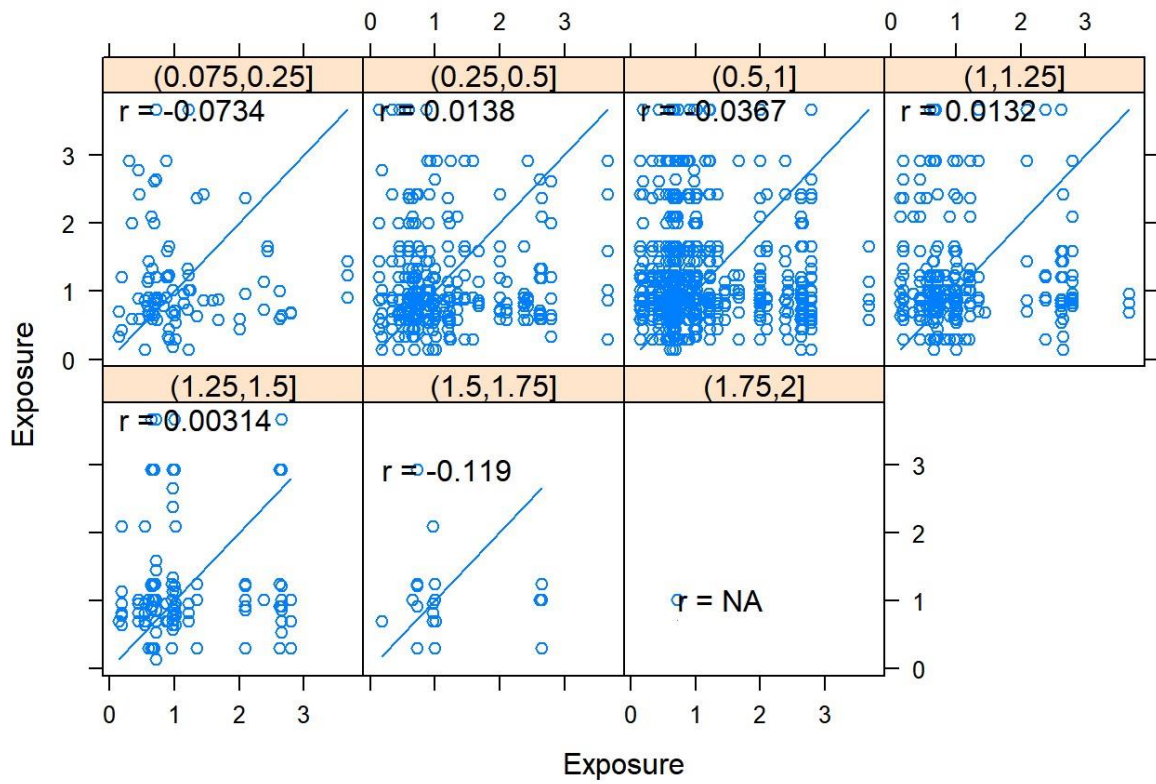


```
coordnames(cbds_sp)
```

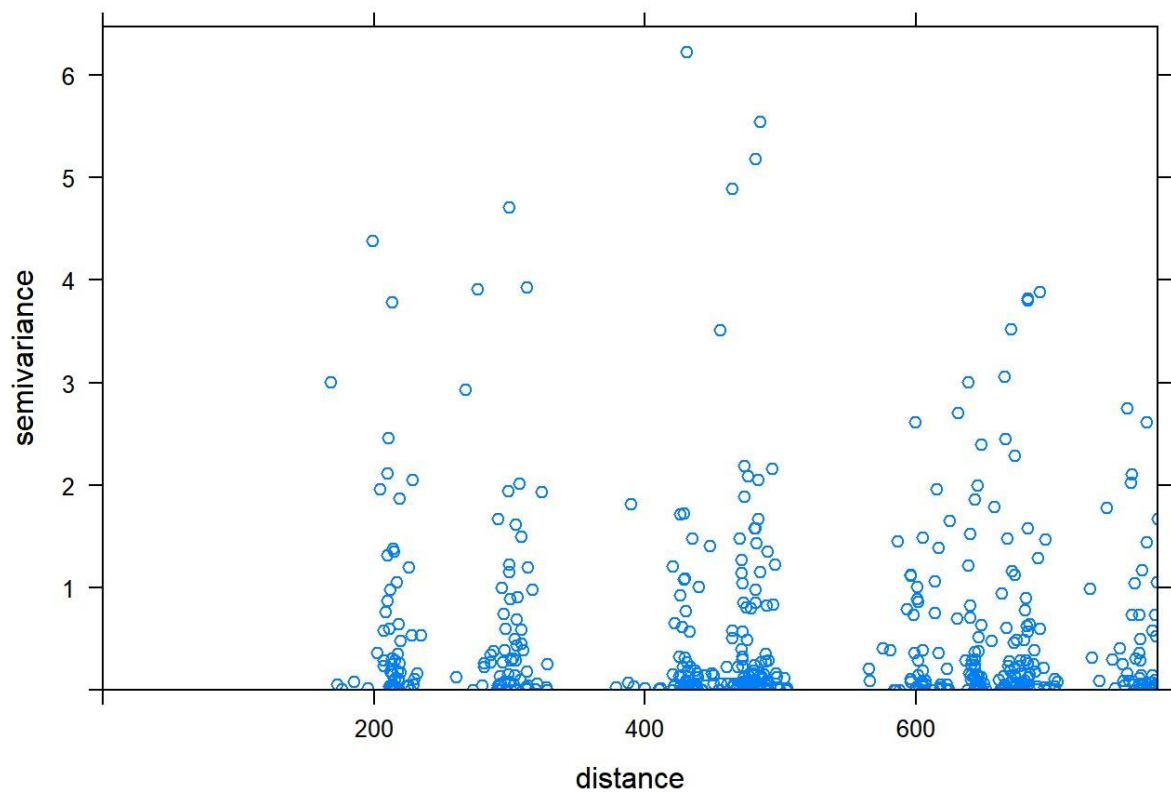
```
## [1] "coords.x1" "coords.x2"
```

```
coordnames(cbds_sp)<- c("x", "y") hscat(Exposure ~1, cbds_sf,  
c(0,0.25,0.5, 0.075,1,1.25,1.5,1.75,2))
```

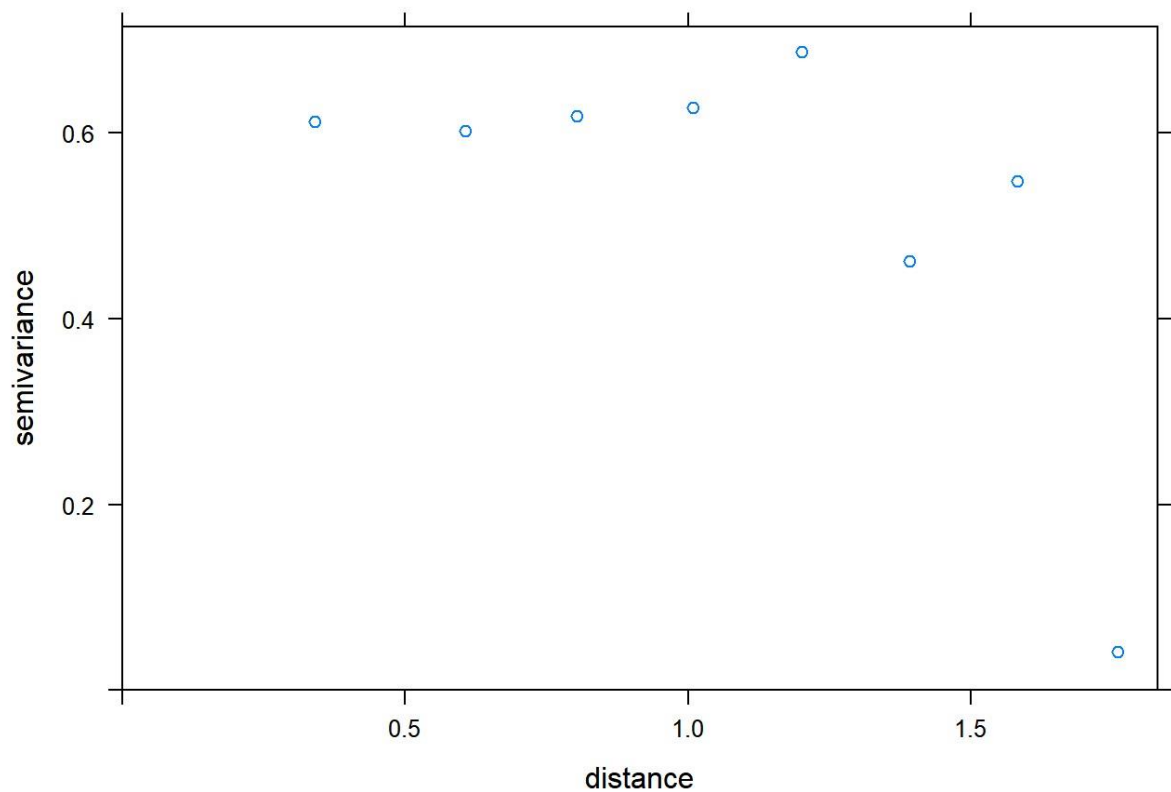
lagged scatterplots



```
#Plotting variogram: expvgm <- variogram(Exposure
~ 1, cbsd_sp, cloud = TRUE) plot(expvgm)
```



```
expvgm <- variogram(Exposure ~ 1, cbds_sf, cloud = FALSE,  
  boundaries = seq(0.5,50,0.2))  
  
plot(expv  
gm)
```



```
vp_model <- fit.variogram(expvgm, model = vgm(
model = "Sph"))
```

```
## Warning in fit.variogram(expvgm, model = vgm(model = "Sph")): singular model in
```

```
## variogram fit
```

```
plot(expvgm, model = vp_model)
```

```
print(vp_model)
```

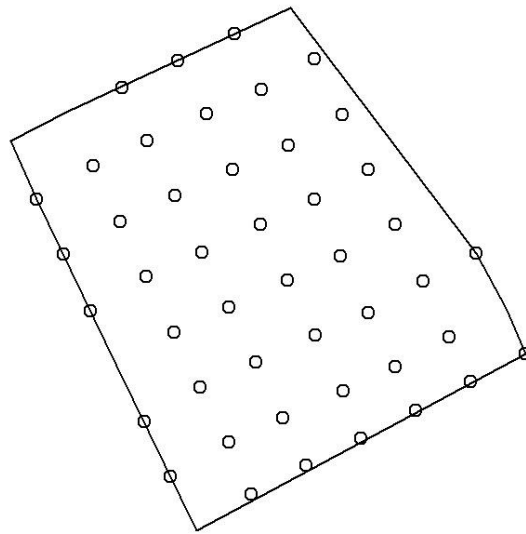
```
## model psill range
```

```
## 1 Sph 0.6126709 0.2877821
```

```
# First in the right projection cbds_perimeter_utm <-
st_transform(cbds_perimeter, crs = 32633)
```

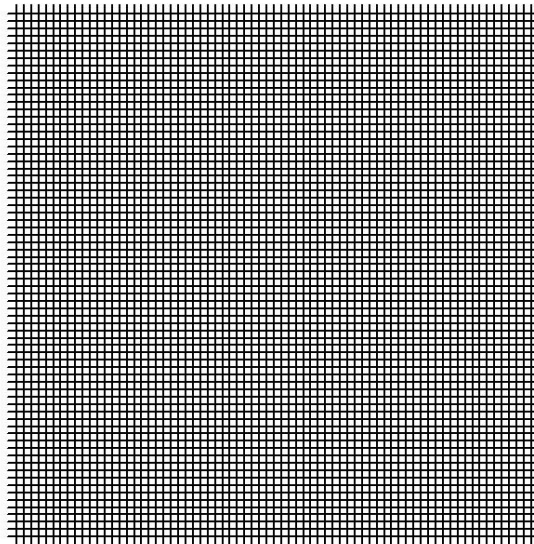
```
# Then to sp compatible type cbd_perimeter_sp <-
as(cbds_perimeter_utm, Class = "Spatial") plot(cbd_perimeter_sp);
```

```
points(cbds_sp)
```

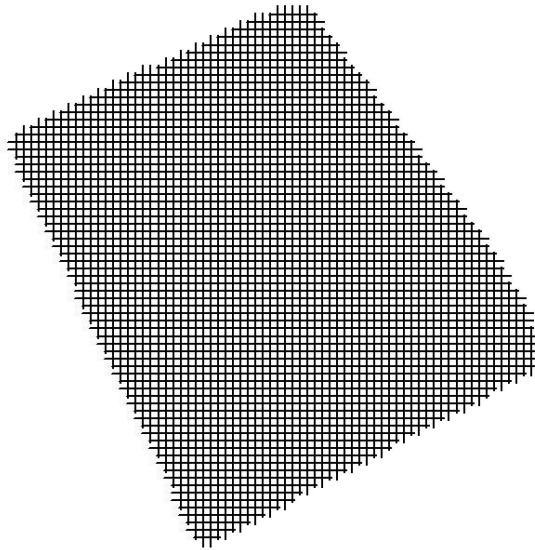


```
bbox_cbds <- bbox(cbd_perimeter_sp)
bbox_cbds
##      min      max
## x 2988089.6 2989883.6
## y -154023.2 -152203.5
# The first parameter is the bottom left corner resolution <- 25 slabel_x <-
as.integer((bbox_cbds[1,2] - bbox_cbds[1,1]) / resolution) slabel_y <-
as.integer((bbox_cbds[2,2] - bbox_cbds[2,1]) / resolution)
cbdsgrid <- GridTopology(c(2988089, -154024), c(resolution, resolution), c(slabel_x,
slabel_y)) library(raster)
```

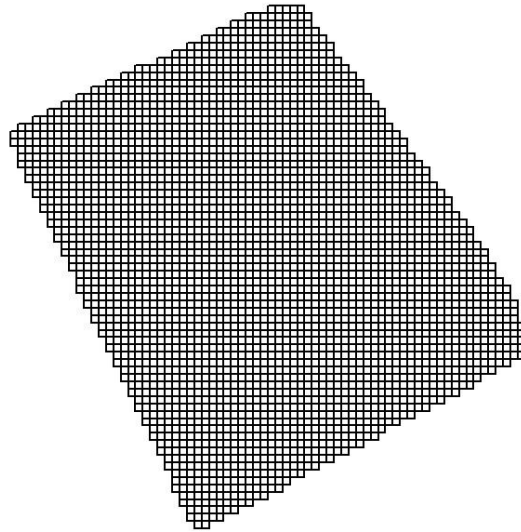
```
##  
## Attaching package: 'raster'  
## The following object is masked from 'package:dplyr':  
##  
## select  
# Create points with the same coordinate system as the boundary  
cbdsgridpoints <- SpatialPoints(cbdsgird, proj4string = CRS(projection(cbd_perimeter_sp))) plot(cbdsgirdpoints)
```



```
cbdsroppedpoints <- crop(cbdsgirdpoints, cbd_perimeter_sp) plot(cbdsroppedpoints)
```



```
cbdsspgrid <- SpatialPixels(cbdscroppedpoints)
coordnames(cbdsgripoints) <- c("x", "y")
plot(cbdsspgrid)
```



```
proj4string(cbdsp)  
proj4string(cbdsp) <- CRS(proj4string(cbdsspgrid))  
## Warning in proj4string(cbdsspgrid): CRS object has comment, which is lost in  
## output  
## Warning in proj4string(obj): CRS object has comment, which is lost in outp ut  
cbdexposuregrid <- krige(Exposure ~ 1, cbdsp, newdata = cbdsspgrid, model =  
vp_model, nmax = 5)  
## [using ordinary kriging]  
#Mapping inteporlated values:  
spplot(cbdexposuregrid, zcol = "var1.pred")
```

```
#Mapping inteporlated values variance:  
spplot(cbdexposuregrid, zcol = "var1.var")
```



```

#Calculating the probability of exposure exceeding IV/m threshold
<- 2
cbdexposuregrid$pExposure <- 1.5 - pnorm(threshold, mean = cbdexposuregrid$va
r1.pred, sd = sqrt(cbdexposuregrid$var1.var)) spplot(cbdexposuregrid, zcol =
"pExposure")

```

```

#Gridded prediction using Inverse Distance Weighting (IDW) idw.out
<- idw(Exposure ~1, cbds_sp, cbdsppgrid, idp = 2.5)
## [inverse distance weighted interpolation]
#Mapping      inteporlated      values
spplot(idw.out, zcol = "var1.pred")

```

```

#Interactive map with satellite base map:
mapview(idw.out.raster, alpha.regions = 0.5, legend = TRUE, map.types = "Esri
.WorldImagery")
## Warning in showSRID(uprojargs, format = "PROJ", multiline = "NO", prefer_p roj
=
## prefer_proj): Discarded ellps WGS 84 in Proj4 definition: +proj=merc +a=63 78137
## +b=6378137 +lat_ts=0 +lon_0=0 +x_0=0 +y_0=0 +k=1 +units=m +nadgrids=@null
## +wktext +no_defs +type=crs
## Warning in showSRID(uprojargs, format = "PROJ", multiline = "NO", prefer_p
roj =
## prefer_proj): Discarded datum World Geodetic System 1984 in Proj4 definiti on
## Warning in showSRID(uprojargs, format = "PROJ", multiline = "NO", prefer_p roj
=
## prefer_proj): Discarded ellps WGS 84 in Proj4 definition: +proj=merc +a=63 78137
## +b=6378137 +lat_ts=0 +lon_0=0 +x_0=0 +y_0=0 +k=1 +units=m +nadgrids=@null
## +wktext +no_defs +type=crs
## Warning in showSRID(uprojargs, format = "PROJ", multiline = "NO", prefer_p roj

```

```
=
```

```
## prefer_proj): Discarded datum World Geodetic System 1984 in Proj4 defin
```

Appendix 2: R Code for PCA

```
library(chemometrics)
```

```
## Loading required package: rpart
```

```
library(ChemoSpecUtils)
```

```
library(ChemoSpec)
```

```
##
```

```
## The ChemoSpec graphics option is set to 'base'
```

```
## To change it, do
```

```
## options(ChemoSpecGraphics = 'option'),
```

```
## where 'option' is one of 'base' or 'ggplot2'
```

```
library(knitr)
```

```
library(R.utils)
```

```
## Loading required package: R.oo
```

```
## Loading required package: R.methodsS3
```

```
## R.methodsS3 v1.8.1 (2020-08-26 16:20:06 UTC) successfully loaded. See ?R.methodsS3 for help.
```

```
## R.oo v1.24.0 (2020-08-26 16:11:58 UTC) successfully loaded. See ?R.oo for help.
```

```
##
```

```
## Attaching package: 'R.oo'
```

```
## The following object is masked from 'package:R.methodsS3':
```

```
##
```

```
## throw
```

```
## The following objects are masked from 'package:methods':
```

```
##
```

```
## getClasses, getMethods
```

```
## The following objects are masked from 'package:base': ##
```

```
## attach, detach, load, save
```

```
## R.utils v2.10.1 (2020-08-26 22:50:31 UTC) successfully loaded. See ?R.utils for  
help.
```

```
##
```

```
## Attaching package: 'R.utils'
```

```
## The following object is masked from 'package:utils':
```

```
##
```

```

##      timestamp
## The following objects are masked from 'package:base':
##
##      cat, commandArgs, getOption, inherits, isOpen, nullfile, parse,
##      warnings
#load the data and make available for analysis
rfemf<-matrix2SpectraObject(gr.crit = c("Residential", "CBD"),
                           gr.cols = c("red", "blue"),
                           freq.unit = "Frequency",
                           int.unit = "Electric Field",
                           descrip = "Radiation Study",
                           in.file = "DataforPCA.csv",
                           chk = TRUE,
                           out.file = "",
                           sep = ",",
                           dec = ".")
##
## Reading 1 file(s)...
##
## Assigning 26 spectra to 2 group(s)...
# summarize the data set to make sure your data are in good shape.
#verify that the data ranges and other details look like as expected
sumSpectra(rfemf)
##
## Radiation Study
##
## There are 26 spectra in this set.
## The y-axis unit is Electric Field.
##
## The frequency scale runs from
## 7.32e+08 to 2.689e+09 Frequency
## There are 296 frequency values.
## The frequency resolution is
## 1436000 Frequency/point.

```

```
##
```

```

## This data set is not continuous ##
along the frequency axis.
## Here are the data chunks:

##
## beg.freq end.freq size beg.indx end.indx
## 1 732000000 862000000 1.30e+08 1 102
## 2 924900000 960000000 3.51e+07 103 148
## 3 1805200000 1877000000 7.18e+07 149 199
## 4 2110500000 2169000000 5.85e+07 200 239
## 5 2546500000 2585500000 3.90e+07 240 266
## 6 2596000000 2606500000 1.05e+07 267 274 ##
7 2657500000 2689000000 3.15e+07 275 296
##

## The spectra are divided into 2 groups:

##
## group no. color symbol alt.sym
## 1 CBD 13 blue 1 b ## 2
Residential 13 red 0 a
##
##

## *** Note: this is an S3 object

## of class 'Spectra'
spe3<-normSpectra(rfemf) pca3<-c_pcaSpectra(spe3, choice
= "noscale", cent = TRUE) #check for gaps to confirm
frequencybands of interest check4Gaps(rfemf$freq,
rfemf$data[5,])

```

```
## beg.freq end.freq size beg.indx end.indx
```

```
## 1 732000000 862000000 1.30e+08 1 102
## 2 924900000 960000000 3.51e+07 103 148
## 3 1805200000 1877000000 7.18e+07 149 199
## 4 2110500000 2169000000 5.85e+07 200 239
## 5 2546500000 2585500000 3.90e+07 240 266
## 6 2596000000 2606500000 1.05e+07 267 274
## 7 2657500000 2689000000 3.15e+07 275 296
```

```
rfe<-normSpectra(rfemf) c_res<-c_pcaSpectra(rfe, choice="noscale", cent =
TRUE) plotScores(rfe, c_res, main="", pcs = c(1,2), ellipse = "none",tol = 0)
```

Splots code

```
spt <- sPlotSpectra(rfemf, c_res, main = "", pc = 1, tol = 0.001)
```

Appendix 3: Summary of CBD Electric Field Values for Various Bands

Position	GSM1800	GSM900	UMTS2100	LTE700	LTE800	LTE2600	Total
1	0.436521	0.744252	0.398614	0.030397	0.006433	0.199812	0.971725
2	0.072649	0.143802	0.060652	0.045054	0.006109	0.032471	0.181012
3	0.043767	0.386592	0.118827	0.123049	0.070587	0.050803	0.433819
4	0.523825	2.720237	0.092504	0.082351	0.263818	0.093551	2.787073
5	0.187901	0.630418	0.097841	0.048108	0.160772	0.061599	0.688672
6	0.087768	2.620159	0.045307	0.036682	0.006433	0.035928	2.622532
7	0.061619	0.974143	0.176243	0.056149	0.112046	0.032801	1.000302
8	0.142414	0.603605	0.169539	0.289307	0.104973	0.076852	0.716936
9	0.124772	2.635865	0.122466	0.118842	0.140378	0.052089	2.648565
10	0.255647	0.324483	0.490892	0.022116	0.10291	0.069287	0.653842
11	0.217229	0.530374	0.091547	0.022509	0.13338	0.040181	0.597315
12	0.117186	0.535561	0.166435	0.105634	0.255883	0.142919	0.652172
13	0.087364	0.623944	0.231656	0.02641	0.082402	0.041242	0.678085
14	0.062435	0.544301	0.312284	0.034431	0.46914	0.439313	0.901091
15	0.039091	1.170666	0.312284	0.015865	0.080518	0.079444	1.217606
16	0.001721	0.826187	0.312284	0.034431	0.232946	0.439313	1.01418
17	0.154969	0.482391	0.143163	0.015865	0.098603	0.067578	0.540147
18	0.032932	0.098093	0.049693	0.027506	0.064833	0.035185	0.139213
19	0.266403	0.064405	0.117922	0.059064	0.135418	0.046165	0.336134
20	1.713909	0.911247	0.350549	0.022614	0.292053	0.114016	1.997385
21	0.327717	0.135967	0.301623	0.137908	0.325927	0.126737	0.598527
22	0.531574	0.758857	0.622542	0.06134	0.361221	0.255503	1.202324
23	0.418194	1.203007	0.297068	0.031746	0.237472	0.139565	1.336903
24	0.266012	0.408425	0.23777	0.044296	0.331822	0.090784	0.643798
25	2.074483	0.149101	0.12746	0.031438	0.219649	0.064476	2.096523
26	0.547405	0.77813	2.117595	0.035689	0.20055	0.461147	2.375618
27	0.331172	0.595229	0.162148	0.100361	0.152263	0.11235	0.732235
28	0.844874	0.011477	0.241846	0.153393	0.13408	0.100544	0.907785
29	0.191179	0.149101	0.248621	0.109439	0.238968	0.105746	0.448198

30	0.307692	0.417225	0.149613	0.052608	0.241481	0.068275	0.597412
----	----------	----------	----------	----------	----------	----------	----------

31	0.149096	0.636892	0.152287	0.111004	0.178231	0.070435	0.707195
32	0.247314	0.815495	0.049596	0.050631	0.153429	0.048234	0.870121
33	1.028347	0.590541	0.066521	0.051632	0.254546	0.06139	1.217339
34	0.482288	1.133224	3.374784	0.061558	0.174134	0.712882	3.667193
35	0.574518	1.21728	0.396	0.042953	0.329705	0.12353	1.447236
36	0.547984	1.564107	1.685544	0.195865	0.22462	0.464952	2.427509
37	0.634425	1.160297	0.90179	0.046301	0.42996	0.182833	1.668068
38	0.198606	0.436465	0.215069	0.041158	0.216069	0.084651	0.575978
39	0.235493	1.090608	0.153104	0.022126	0.170643	0.071929	1.141537
40	0.183509	0.912323	0.163567	0.022998	0.175143	0.057897	0.963008
41	0.282441	0.456536	0.366201	0.108504	0.179907	0.130053	0.69529
42	0.738879	0.272727	0.172566	0.040202	0.131779	0.082036	0.822118
43	0.206313	0.725942	0.150706	0.035594	0.121216	0.064441	0.782591
44	0.143751	0.82553	0.111054	0.042932	0.234435	0.06097	0.880388
45	1.29199	0.883209	0.163773	0.039207	0.201036	0.087027	1.589246
46	0.111108	0.574939	0.489354	0.019341	0.398043	0.061531	0.863147
47	0.520291	0.730748	0.093651	0.034916	0.14745	0.051849	0.916064
48	0.720901	0.872708	0.342374	0.037364	0.356167	0.146738	1.244339
49	0.431251	0.434641	0.386091	0.027615	0.699489	0.147273	1.017719
50	0.098962	0.176575	0.205514	0.033183	0.041158	0.049985	0.297532
51	1.200326	1.360944	2.261519	0.032325	0.15727	0.326119	2.922255
